PRODUCTION OF ACTIVATED CARBONACEOUS CATALYST FOR THEIR APPLICATION IN BIO JET-FUEL SYNTHESIS

Miss Araya Smuthkochorn

A Thesis Submitted in Partial Fulfillment of the Requirements
for the Degree of Master of Engineering in Chemical Engineering
Department of Chemical Engineering
FACULTY OF ENGINEERING
Chulalongkorn University
Academic Year 2019

การผลิตตัวเร่งปฏิกิริยาชนิดคาร์บอนกัมมันต์สำหรับประยุกต์ใช้ในการสังเคราะห์น้ำมันอากาศยานชีวภาพ

น.ส.อารยา สมุทรโคจร

วิทยานิพนธ์นี้เป็นส่วนหนึ่งของการศึกษาตามหลักสูตรปริญญาวิศวกรรมศาสตรมหาบัณฑิต
สาขาวิชาวิศวกรรมเคมี ภาควิชาวิศวกรรมเคมี
คณะวิศวกรรมศาสตร์ จุฬาลงกรณ์มหาวิทยาลัย
ปีการศึกษา 2562

Thesis Title	PRODUCTION OF ACTIVATED CARBONACEOUS CATALYST FOR THEIR APPLICATION IN BIO JET-FUEL SYNTHESIS
By	Miss Araya Smuthkochorn
Field of Study	Chemical Engineering
Thesis Advisor	Associate Professor Dr. TAWATCHAI CHARINPANITKUL
Thesis Co Advisor	Dr. Kajornsak Faungnawakij

Accepted by the FACULTY OF ENGINEERING, Chulalongkorn University in Partial Fulfillment of the Requirement for the Master of Engineering

..... Dean of the FACULTY OF ENGINEERING
(Professor Dr. SUPOT TEACHAVORASINSKUN)

THESIS COMMITTEE

..... Chairman
(Professor Dr. SARAWUT RIMDUSIT)

..... Thesis Advisor
(Associate Professor Dr. TAWATCHAI CHARINPANITKUL)

..... Thesis Co-Advisor
(Dr. Kajornsak Faungnawakij)

..... Examiner
(Dr. CHALIDA KLAYSOM)

..... External Examiner
(Assistant Professor Dr. APILUCK EIAD-UA)

อารยา สมุทรโคจร : การผลิตตัวเร่งปฏิกิริยาชนิดคาร์บอนกัมมันต์สำหรับประยุกต์ใช้ในการสังเคราะห์น้ำมันอากาศยานชีวภาพ . (PRODUCTION OF ACTIVATED CARBONACEOUS CATALYST FOR THEIR APPLICATION IN BIO JET-FUEL SYNTHESIS) อ.ที่ปรึกษาหลัก : รศ. ดร.ธวัชชัย ชรินพาณิชกุล, อ.ที่ปรึกษาร่วม : ดร.ขจรศักดิ์ เฟื่องนวกิจ

ในปัจจุบันการพัฒนางานวิจัยด้านพลังงานทางเลือกเพื่อทดแทนพลังงานที่ได้จากเชื้อเพลิงฟอสซิลได้รับความสนใจจากทีมวิจัยจำนวนมาก กระบวนการไฮโดรดีออกซิจีเนชันเป็นหนึ่งในกระบวนการที่มีประสิทธิภาพสูงสุดในการผลิตเชื้อเพลิงจากชีวมวล ในงานวิจัยนี้ได้ทำการสังเคราะห์คาร์บอนกัมมันต์จากน้ำมันด้อยคุณภาพด้วยกระบวนการคาร์บอไนเซชันและกระบวนการกระตุ้นทางเคมี เพื่อประยุกต์ใช้เป็นตัวรองรับตัวเร่งปฏิกิริยา คาร์บอนกัมมันต์ที่สังเคราะห์ขึ้นมีพื้นที่ผิวสูง 1527.4 ตารางเมตรต่อกรัม ซึ่งได้จากกระบวนการกระตุ้นร่วมกับโพแทสเซียมไฮดรอกไซด์ในอัตราส่วน 1:1 และกระบวนการคาร์บอไนเซชันที่อุณหภูมิ 700 องศาเซลเซียส ตัวเร่งปฏิกิริยาโมลิบดีนัมฟอสไฟด์บนตัวรองรับคาร์บอนกัมมันต์ถูกเตรียมขึ้นด้วยกระบวนการเคลือบฝัง โดยตัวเร่งปฏิกิริยาที่เตรียมขึ้นมีการกระจายตัวของอนุภาคโลหะโมลิบดีนัมฟอสไฟด์บนตัวรองรับคาร์บอนกัมมันต์อย่างเป็นระเบียบ และเมื่อนำตัวเร่งปฏิกิริยาไปใช้ในกระบวนการไฮโดรดีออกซิจีเนชันของน้ำมันพืช พบว่า ตัวเร่งปฏิกิริยาที่ได้จากกระบวนการเคลือบฝังโลหะโมลิบดีนัมฟอสไฟด์ในปริมาณร้อยละ 5 และการทำปฏิกิริยาที่อุณหภูมิ 420 องศาเซลเซียสเป็นตัวเร่งปฏิกิริยาที่มีความสามารถในการทำปฏิกิริยาสูงสุด ซึ่งเปลี่ยนน้ำมันพืชได้ร้อยละ 100 โดยผลิตภัณฑ์ที่ได้เป็นสัดส่วนของกรีนดีเซลและน้ำมันอากาศยาน ร้อยละ 9.6 และ 90.4 ตามลำดับ นอกจากนี้ตัวเร่งปฏิกิริยาดังกล่าวยังมีประสิทธิภาพในการใช้งานในระยะยาวถึง 12 ชั่วโมง โดยไม่มีการเสื่อมสภาพของตัวเร่งปฏิกิริยาอีกด้วย

สาขาวิชา	วิศวกรรมเคมี	ลายมือชื่อนิสิต .....
ปีการศึกษา	2562	ลายมือชื่อ อ.ที่ปรึกษาหลัก .....
		ลายมือชื่อ อ.ที่ปรึกษาร่วม .....

6170338421 : MAJOR CHEMICAL ENGINEERING
KEYWOR D: activation, carbonization, catalyst, hydrodeoxygenation

Araya Smuthkochorn : PRODUCTION OF ACTIVATED CARBONACEOUS CATALYST FOR THEIR APPLICATION IN BIO JET-FUEL SYNTHESIS. Advisor: Assoc. Prof. Dr. TAWATCHAI CHARINPANITKUL Co-advisor: Dr. Kajornsak Faungnawakij

Recently, research and development in alternative aviation fuel to replace fossil-based fuel has been of interest for many research works. Hydrodeoxygenation (HDO) is one of the most efficient processes to produce clean fuel. This study involves the synthesis of activated carbon (AC) from heavy fuel oil (HFO) via the carbonization-chemical activation process for utilization as catalyst support. AC with a high surface area of 1527.4 m^2/g was obtained from KOH-activation in the ratio of 1:1 and carbonization temperature of 700°C. The molybdenum phosphide (MoP) catalyst impregnated on AC was prepared via the wet impregnation process. The microscopic analysis revealed the uniform dispersion of MoP nanoparticles on AC. The performance of the catalyst was evaluated by the HDO of palm oil to produce jet fuel. The MoP loading of 5 wt% and reaction temperature of 420°C could provide the resultant catalyst with the best activity, resulted in oil conversion of 100%. The typical liquid HC product contained 9.6 and 90.4% of green diesel and bio jet-oil, respectively. Furthermore, the catalyst presented good stability even employed for 12 h without significant deactivation.

Field of Study:	Chemical Engineering	Student's Signature .....
Academic Year:	2019	Advisor's Signature .....
		Co-advisor's Signature .....

ACKNOWLEDGEMENTS

First, I would like to thank the Department of Chemical Engineering, Faculty of Engineering, Chulalongkorn University, College of Nanotechnology, King Mongkut's Institute of Technology Ladkrabang, and National Nanotechnology Center (NANOTEC), National Science and Technology Development Agency (NSTDA) for contribution to this research.

Secondly, I would like to express my sincere appreciation to my advisor, Associate Professor Dr. Tawatchai Charinpanitkul, for his support, suggestion, and leading me to do this worthwhile project. I want to express my special thanks to my co-advisor, Dr. Kajornsak Faungnawakij, for his suggestion, and valuable information. I want to express my gratitude to Assistant Professor. Dr. Apiluck Eaid-Ua for his support, and advice, since being an undergraduate student.

Thirdly, I wish to thank my family and friends for their love, support, encouragement, and sharing of my problems while doing this project.

Finally, I wish to acknowledge the Thailand Graduate Institute of Science and Technology Scholarship, TGIST (TG-55-09-61-065M), for the financial support for this project.

Araya Smuthkochorn

TABLE OF CONTENTS

Page

LIST OF TABLES

LIST OF FIGURES

CHAPTER 1
INTRODUCTION

1.1 Motivation of this research work

Nowadays, energy consumption for transportation dramatically increases, while fossil fuel reserves are limited and tend to decrease continuously. Besides, the combustion of fossil fuel is a significant cause of greenhouse gas (GHG) emission, which affects global warming [1, 2]. Meanwhile, air transportation is vital in the global economy and society, resulting in the rapidly increasing demand of jet fuel. The International Air Transport Association (IATA) creates a GHG emissions reduction roadmap to decline the environmental impact of air transportation by improving fuel efficiency of 1.5% per year through 2020 [3]. Lending to the search for alternative energy resources to replace fossil fuel, bio-based fuel with similar compositions of fossil-based fuel is considered as sustainable alternative drop-in fuel [4, 5]. It commonly advocates as a cost-effective and environment-friendly with lowers GHG emission and lower toxic gas production [6].

Biofuels could be derived from renewable energy resources, such as plants and animals [7], which can produce through pyrolysis, transesterification, and hydrodeoxygenation (HDO), etc [8, 9]. It could be categorized into three types, including primary, secondary, and tertiary biofuels. In general, vegetable oil, animal fats, lignocellulosic materials, and algae oil could be used as a source for such biofuels [6, 9]. The release of carbon dioxide (CO_2) from the combustion of biofuels merely returns to atmospheric CO_2, which plants use in the photosynthesis process. Therefore, biofuels are a beneficial means for reducing CO_2 emission, at least at first sight [2]. However, biofuels have low oxidative stability, low cold flow properties, and low energy density due to the presence of oxygen atoms and unsaturated carbon bonds [10]. Hydrodeoxygenation (HDO) is the most efficient process for biofuels production, which provides high-quality fuel suitable for use in diesel engines [11].

HDO process consists of three main reactions, including decarboxylation (DCO_2), decarbonylation (DCO), and hydrodeoxygenation (HDO), which generates

CO_2, CO, and H_2O as a by-product, respectively [10, 11]. Vegetable oil and animal fat compose of triglycerides are subjected to catalytic HDO process with high H_2 pressure and moderate temperature to produce a renewable jet, and green diesel fuel [12]. Starting with hydrogenation of unsaturated triglycerides to saturated triglycerides and hydrogenolysis to fatty acids, deoxygenation of fatty acids could provide n-alkanes [3]. Several catalysts employed in this process are noble metal (i.e., Pd and Pt) embedded on silicon dioxide, aluminum oxide, and activated carbon (AC) [13, 14]. Among various support materials, AC is the most efficient for the HDO process due to a high surface area, large porosity, and good metal catalyst dispersion [15]. Surface characteristics of the support enhances the product yield and preserves the catalyst deactivation via coke formation [16]. Hence, the development of a combination of metal catalyst and stable support material for HDO is crucial in the production of high-quality bio-based fuel.

AC can produce from renewable and low-cost materials, such as agriculture wastes and industrial residues [17]. Such a venture would help contribute to waste elimination and add value to waste. In the oil industry, slop oil is one of the present waste streams [16]. It considers as a multi-component mixture of hydrocarbons (e.g., alkane, cycloalkane, and aromatic), water and, sludge. Therefore, it could fractionate into various fractions, such as light oil, middle oil, and heavy oil, etc [18]. Due to its high-carbon content, slop oil can use as an AC feedstock.

The carbonization process uses high thermal energy (400 to 900°C) to convert organic materials into carbonaceous products, which depends on the starting materials [19]. High surface characteristics of AC, including surface area, and pore volume are needed for HDO reaction, which can enhance by the impregnation of carbonaceous materials with any chemicals such as H_3PO_4, $ZnCl_2$, NaOH, and KOH, etc. [20, 21]. A well-disperses metal catalyst on AC's surface and sufficiently reaction parameters require to reach a high yield of biofuels production.

The production of AC from heavy fuel oil (HFO) for utilization as a MoP catalyst support in HDO of vegetable oil to bio jet-oil is crucially interested. In this study, AC was prepared using a one-step process of carbonization-chemical activation, using potassium hydroxide (KOH) as an activating agent. The resultant AC was

characterized based on proximate and ultimate analysis, scanning electron microscopic (SEM) analysis, Nitrogen adsorption-desorption (N_2-sorption) analysis, and Fourier transform infrared spectroscopic (FTIR) analysis. MoP catalyst impregnated on AC was prepared by the wet impregnation process, using ammonium molybdate $(NH_4)_6Mo_7O_{24}$ and di-ammonium hydrogen phosphate $(NH_4)_2HPO_4$ as a precursor. Synthesized MoP catalyst on AC support was characterized by Scanning electron microscopic-Energy dispersive spectrometry (SEM-EDS) analysis, Transmission electron microscopic (TEM) analysis, Nitrogen adsorption-desorption (N_2-sorption) analysis, X-ray diffraction (XRD) analysis, Ammonia temperature-programmed desorption (NH_3-TPD) analysis, and Hydrogen temperature-programmed reduction (H_2-TPR) analysis. A custom-made continuous flow trickle-bed reactor was used to test the catalytic activity. Performance of the MoP impregnated on AC catalyst was analyzed with regard to oil conversion, liquid HC yield, green diesel, and bio jet-oil selectivity. The effects of metal phosphide loading and reaction temperature in the HDO reaction was also investigated. Deoxygenated product was examined under the control conditions to verify oxidative stability, clod flow properties, and energy density of the synthesized biofuel.

1.2 Research objectives

This research work aimed to produce high surface area AC from HFO, using the carbonization-chemical activation process for utilization as MoP catalyst support for HDO of vegetable oil. The effect of metal phosphide loading and reaction temperature on the performance of as-prepared catalysts was investigated.

1.3 Scope of this research work

The scope of this study was to utilize HFO, which could be recognized as a fraction of slop oil, to produce AC used as a MoP catalyst support. MoP catalyst impregnated on AC was employed for hydrotreating of vegetable oil to synthesize bio jet-oil. This thesis consisted of three main parts, the synthesis of AC via the carbonization-chemical activation process, preparation of MoP catalyst impregnated on AC by wet impregnation process, and investigation of the effect of metal phosphide loading and reaction temperature on the performance of as-prepared catalysts in HDO reaction. Accordingly, the conceptual plan of those parts was deliberated as follows,

1.3.1 Synthesis of activated carbon

Synthesis of AC from HFO by carbonization with various carbonization temperatures (400, 500, 600, and 700°C), and KOH activation with different activating agent ratios (0.5, 1, 1.5, and 2). Characterization of as-prepared AC by production yield, proximate and ultimate analysis, SEM, N_2-sorption, and FTIR.

1.3.2 Preparation of metal catalyst impregnated on AC

Preparation of MoP catalyst impregnated on AC by wet impregnation with various metal phosphide loading (5, 10, 15, and 20 wt%). Characterization of as-prepared catalysts by SEM-EDS, TEM, N_2-sorption, XRD, NH_3-TPD, and H_2-TPR techniques.

1.3.3 Reaction study in HDO process

Examined the effect of metal phosphide loading (5, 10, 15, and 20 wt%) and reaction temperatures (400, 420, and 440°C) for HDO of vegetable oil to produce bio jet-oil using an as-prepared catalyst. Characterization of deoxygenated products by GCMS, to investigate oil conversion, liquid HC yield, green diesel, and bio jet-oil selectivity.

1.4 Implementation plan

I have followed eight steps to conduct in this work as shown in Table 1.1

1.4.1 I conducted a literature reviewed with a focus on the production of AC as a catalyst support and HDO reaction.

1.4.2 I carried out the synthesis and characterization of AC from HFO via the carbonization-chemical activation process.

1.4.3 I prepared a proposal examination.

1.4.4 I conducted the preparation and characterization of the MoP catalyst impregnated on AC via the wet impregnation process.

1.4.5 I studied the HDO reaction of vegetable oil using an as-prepared catalyst within a custom-made continuous flow trickle-bed reactor.

1.4.6 I made a discussion of all experimental results and made conclusions.

1.4.7 I prepared a manuscript to publish in a SCOPUS journal.

1.4.8 I wrote a thesis book and prepared a thesis defending examination.

Table 1.1 Implementation plan

Activity	Monthly (2019)												Monthly (2020)				
	1	2	3	4	5	6	7	8	9	10	11	12	1	2	3	4	5
Conduct a literature review																	
Carry out synthesis and characterization of AC																	
Prepare proposal examination																	
Conduct preparation and characterization of MoP catalyst																	
Study HDO reaction																	
Make discussion of experiment results and made conclusions																	

Prepare manuscript to publish in the SCOPUS journal																	
Write thesis book and prepared thesis defending examination																	

1.5 Expected benefit

Understanding and knowledge of the production of AC and MoP catalyst impregnated on AC using carbonization-chemical activation and wet impregnation process would be obtained.

Besides, the know-how of the applying of as-prepared catalysts in the HDO reaction would also be obtained.

Know-how of the liquidation of industrial waste, such as slop oil, would also be investigated, reported to reduce its destruction cost, and expands its added value.

CHAPTER 2
FUNDAMENTAL KNOWLEDGE

In order to produce activated carbon (AC) form heavy fuel oil (HFO) for employment as molybdenum phosphide (MoP) catalyst support in hydrodeoxygenation (HDO) process, basic knowledge and understanding are essential. Hence, basic knowledge of biofuel technology, hydrodeoxygenation (HDO) reaction, heterogeneous catalysis, activated carbon (AC), and characterization techniques were described in this chapter.

2.1 Biofuel technology

Biofuel is a fuel derived from biomass, which can be burned directly or mixed with conventional fuels. Since such feedstock materials can be readily replenished, biofuel is considered a renewable energy resource, which is a cost-effective and environmentally friendly fuel. Based on feedstock and method of production, biofuel is classified into three groups named as first, second, and third-generation biofuel [22]. First-generation or conventional biofuel is directly derived from food crops, for example, the bioethanol produced from the fermentation of sugar and starch. However, the first-generation biofuel still has a problem due to the increase in demand for food crops, resulting in an increase in food prices [6]. Second-generation biofuel has been developed to overcome a limitation of the first-generation biofuel. The second-generation biofuel is derived from lignocellulosic materials, for example, the synthetic diesel produced from the hydrotreating of vegetable oil (e.g., palm oil and soybean oil, etc.). It is typically blended with petroleum diesel in various ratios, which can be used in diesel engines [9]. Lastly, third-generation biofuel is manufactured from algae, which is a low cost, high energy, and entirely renewable feedstock. The algae-based biofuel can be produced into a wide range of fuel, such as petrol, diesel, and jet fuel. However, there also has a problem with commercial production, which is in the development process [8].

2.2 Hydrodeoxygenation reaction

Hydrodeoxygenation (HDO) reaction is the most efficient process for biofuel production, which effective in unsaturated bonds and oxygen atoms removal. This process operates under the H_2 atmosphere at high pressure (2-15 MPa) and moderate temperature (350-450°C). **Fig. 2.1** shows a stoichiometric reaction of the conversion of triglycerides to clean fuel. Starting from the hydrogenation of unsaturated triglycerides to saturated triglycerides, then hydrogenolysis to fatty acids and propane. After that, oxygen compounds in fatty acids are cleaved by the deoxygenation, which includes three main reactions are named hydrodeoxygenation (HDO), decarboxylation (DCO_2), and decarbonylation (DCO). In this process, the oxygen atoms are eliminated in the form of H_2O, CO_2, and CO, respectively during the HDO reaction, hydrocarbons are formed with the same number of a carbon atom as original fatty acids. Meanwhile, in the DCO_2 and DCO reaction, hydrocarbons are formed one less carbon atom than precursor fatty acids. At the end of the process, liquid hydrocarbons are produced as the constitutes of gasoline, jet fuel and, green diesel, which is used either pure or mixed with fossil fuel in diesel engines [16]. Several types of catalyst used in this process are commercial hydrotreatment catalyst, such as noble metal (e.g., Pd, Pt, Ru, and Rh, etc.) supported on porous material (e.g., silica, alumina, and activated carbon, etc.) [13, 14]. Besides, the metal catalyst will promote the hydrogenation reaction, while the acidic support will drive the deoxygenation reaction.

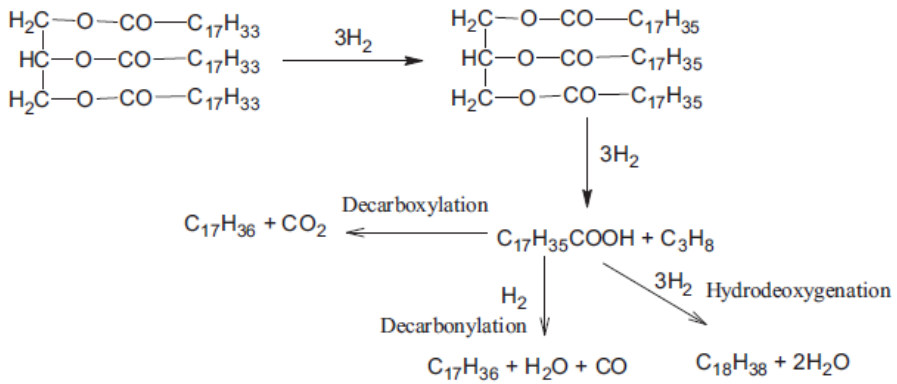

Figure 2.1 Stoichiometric reaction in the conversion of triglycerides to green diesel, adopted from [16]

2.3 Heterogeneous catalyst

Heterogeneous catalysis is a type of catalysis in which the catalyst occupies a different phase from the reactants and products. The great majority of heterogeneous catalysis is a solid catalyst and a liquid or gas reactant. The advantage of such catalysis is easy to separate from reaction mixtures. Besides, the catalyst also consists of two main parts, the first part is called the active phase, which site that reaction occurs, such as metal, metal oxide, metal sulfide, and metal phosphide, etc. The second part is called the support phase, which sites that active phase disperses, which are porous materials. **Table 2.1** collected various supporting materials used as catalyst support, including activated carbon, zeolites, silica gels, activated clay, and activated alumina. Such porous materials have a high surface characteristic, which will achieve a proper distribution of the metal active phase.

Table 2.1 BET surface area, pore volume and pore diameter of various supporting materials [16]

Support	BET area (m^2/g)	Pore volume (cm^3/g)	Pore diameter (nm)
Activated carbon	500-1500	0.6-0.8	0.6-2
Zeolites	500-1000	0.5-0.8	0.4-1.8
Silica gels	200-600	0.04	3-20
Activated clay	150-225	0.4-0.5	6-40
Activated alumina	100-300	0.4-0.5	6-40

In heterogeneous catalysis, the reactant is diffused and adsorbed to the surface and porosity of the catalyst, forming a chemical bond. 0.4-0.5After the reaction, the product is desorbed and spread away from the catalyst. For the solid catalyst, the surface area and pore volume are also important factors that affect active phase distributions and catalytic activity. Hence, the development of the catalyst is an important key to enhance catalytic performance and protect catalyst deactivation [16].

2.4 Activated carbon

Activated carbon (AC) or activated charcoal is a carbonaceous material, which has a high surface area and large porosity. Generally, it can be found in three primary

forms, including powder, granular, and pellet form, but the most frequently used is a powder form. AC is usually produced from carbon-based materials, such as agricultural waste and industrial residue, through the conventional process (i.e., carbonization-activation). **Table 2.2** collected many materials (i.e., soft wood, hard wood, lignin, nutshells, lignite, soft coal, petroleum coke, semi-hard coal, and hard coal.), which has a high carbon content and low ash content, which is suitable for AC production. Owing to its surface characteristic, AC can be used in various applications, such as adsorbent materials, separation materials, catalyst supporting materials, and electronic devices. Moreover, both physical and chemical activation process increases the surface properties of AC, which enhances the adsorption ability of such material [23].

Table 2.2 Characteristics of carbon-based materials used in the manufacture of AC [23]

Raw material	Carbon (mass %)	Volatiles (mass %)	Density (cm^3/g)	Ash (mass %)	Texture of AC
Soft wood	40-45	55-60	0.4-0.5	0.3-1.1	Soft, Large pore volume
Hard wood	40-42	55-60	0.55-0.8	0.3-1.2	Soft, Large pore volume
Lignin	35-40	59-60	0.3-0.4	-	Soft, Large pore volume
Nutshells	40-45	55-60	1.4	-	Hard, Large micropore volume
Lignite	55-70	25-40	1.0-135	5-6	Hard, small pore volume
Soft coal	65-80	20-30	12.5-1.5	2-12	Medium-hard, medium pore volume
Petroleum coke	70-85	15-20	1.35	0.5-0.7	Medium-hard, medium pore volume
Semi-hard coal	70-75	10-15	1.45	5-15	Hard, Large pore volume
Hard coal	85-95	5-15	1.5-1.8	2-15	Hard, Large pore volume

2.5 Activated carbon production

In general, the method commonly used for the production of activated carbon (AC) is a two-steps process, namely pyrolysis and activation process. Starting from the pyrolysis process, which method for converting organic materials to carbonaceous products follows by the activation process, which means to improve the surface characteristics of AC.

Pyrolysis is a process for decomposing organic materials under an oxygen-free condition in a temperature range 300-900°C. Typically, products obtained from this process are solid, liquid, and gasses. The solid and liquid products are referred to as char and bio-oil, respectively, whereas the gases mixture containing CO, CO_2, H_2, and C_{1-2} hydrocarbons. Besides, the yield of pyrolysis products is depended on the characteristic of raw materials and pyrolysis process adapted. The char product is received at a low heating rate and low temperature. This process provides mostly carbon substance, which is called carbonization process. In contrast, the gas product is found at a high heating rate and high temperature, while the oil product is found at a moderate temperature. Moreover, the increase in temperature leads to the increase in carbon and ash content, while moisture and volatile matter content decrease [24].

Physical activation, also called gas activation is a process that uses gas, such as stream, CO_2 and, ozone, to activate carbonaceous materials at a temperature above 600°C. This process is divided into two-steps, which the carbonization of organic materials to form char. Then partially gasification of resulting char by an oxidant gas to produce AC. The AC obtained from this process has a high surface area and large pore volume, which can be used in various applications [25].

Chemical activation is a process that uses chemical reagents, such as acid (e.g., HCl, H_2SO_4, and H_3PO_4, etc.), base (NaOH and KOH, etc.) or salt ($ZnCl_2$, etc.) to activate carbonaceous materials. The carbonization and activation process occur simultaneously, which is considered as a one-step process. The carbonaceous materials are impregnated with some chemicals, then carbonization at a temperature range 400-900°C to produce AC. The AC obtained from this process has a high surface area with

large micropore volume. Besides, the chemical activation is more preferred than the physical activation due to the shorter time, higher yield and, higher microporosity [26].

2.6 Pore characteristic of activated carbon

The pore classification is an essential requirement of the characterization of porous materials. International Union of Pure and Applied Chemistry (IUPAC) divides porous materials according to the pore diameter into three categories as follows [27],

Microporous material is materials that have a pore diameter greater than 50 nm.

Mesoporous material is materials that have a pore diameter between 2 to 50 nm.

Macroporous material is materials that have a pore diameter greater than 50 nm.

The nitrogen physisorption technique is used to analyze surface properties (e.g., surface area, pore diameter, and pore volume) of porous materials. This technique provides information between volume adsorbate (V_m) and relative pressure (P/P_0) at a constant temperature (-196ºC). The curve that shows such a relationship is also called "Isotherm", displayed in **Fig. 2.2**. The isotherm is classified by IUPAC based on the mechanism occurs in the pore during the adsorption into six types as follows [28],

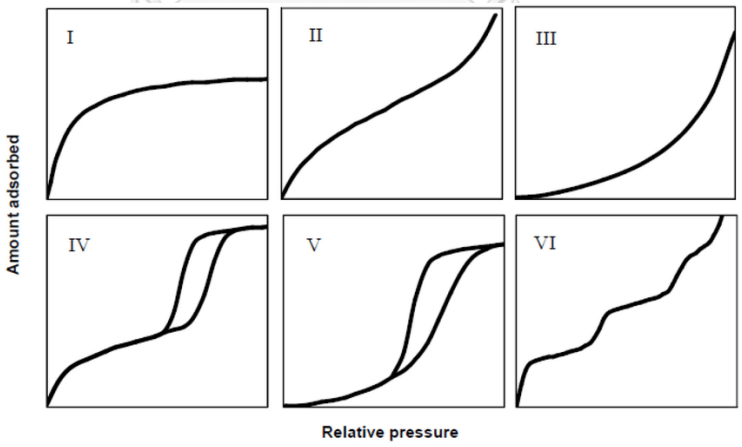

Figure 2.2 Type of adsorption-desorption isotherm according to the IUPAC classification [29]

Type I is the isotherm for monolayer adsorption or Langmuir, which is the easiest one. Monolayer adsorption is the adsorption phenomena of microporous materials, such as activated carbon and zeolite. It can be found both physical and

chemical adsorption process. The quantity of adsorption will rapidly increase with relative pressure increase. Besides, at relative pressure near one, the amount of adsorption will be constant.

Type II is a S-shaped isotherm, usually occurs with non-porous and macroporous materials, which has inflection or knee point. The knee point is a point that the adsorbent surface is completely covered by monolayer adsorption. When the pressure increases, the adsorption process will occur more than one layer. Hence, this type of adsorption is called multilayer adsorption.

Type III is the isotherm that has a similar shape as type II isotherm, without knee point. This isotherm usually occurs with weak adsorption, which is the adsorption of non-porous or macroporous materials.

Type IV is the isotherm that can be found in mesoporous materials. In the first stage of adsorption, the isotherm curve at low relative pressure shows the type II isotherm characteristic. After that, the adsorption will sharply increase with relative pressure increase. This is due to the capillary condensation in the pore structure, which causes a hysteresis loop in the desorption.

Type V is the isotherm that has a similar shape as type IV isotherm. This isotherm usually occurs with weak adsorption, which is the adsorption of non-porous or macroporous materials. The difference is the presence of the hysteresis loop due to the pore condensation at high relative pressure.

Type VI is a multistep isotherm, which is rarely found. It is usually found in the layer by layer adsorption phenomena. Moreover, the shape of isotherm depends on the pressure and adsorption temperature.

2.7 Characterization techniques

2.7.1 Proximate analysis

The proximate analysis provides the composition of materials, including moisture, volatile matter, ash, and fixed carbon, which characterized using a thermogravimetric analyzer. In this technique, the sample was placed in an electronic microbalance and heated up to the desired temperature under a specific atmosphere. The TGA apparatus was continuously recorded the weight of materials as the temperature change. The moisture, volatile matter, and ash content was determined by

ASTM D2867-99, ASTM D6832-98, and ASTM D2866-94, respectively. Whereas, the fixed carbon content was calculated by subtracting from other compositions [30].

2.7.2 Ultimate analysis

The ultimate analysis provides the elemental composition of materials including, carbon (C), hydrogen (H), nitrogen (N), and oxygen (O), which determined using an elemental analyzer. In this technique, the sample was placed in a furnace and burned out at 1000ºC under an oxygen atmosphere. Gas products obtained from the combustion, such as CO_2, H_2O, and N_2 was passed through a detector to measure the C, H, and N content, respectively. Besides, the O content was directly calculated by the difference of all compositions from 100% [31].

2.7.3 Scanning electron microscopic-Energy dispersive spectrometry (SEM-EDS) analysis

Scanning electron microscopic (SEM) analysis used high-energy electron scanned the sample surface. The generated signal between electrons and atoms revealed the sample's information, such as external morphology and phase compositions. This technique can also be analyzed the specific elemental composition of the sample, which was useful for qualitative and quantitative analysis. The energy dispersive spectrometry (EDS) analysis used the X-ray spectrum, which was produced from the scan area of the SEM to identify the elemental composition. The X-ray's energy level, which was specific for each element, was measured by EDS software to investigate the symmetry and their relative proportion.

2.7.4 Transmission electron microscopic (TEM) analysis

The transmission electron microscopic (TEM) analysis used a high-energy electron passed through the thin sample, which is less than 100 nm. The generated signal from the interaction between electrons and atoms provided morphology and phase compositions of the sample. The crystal structure and other features, such as crystal dislocation and crystal grain boundary can be observed. Moreover, this technique can be identified as the elemental composition of the sample using an Energy dispersive spectrometry (EDS) analysis, the same as the SEM technique.

2.7.5 N_2 adsorption/desorption (N_2-sorption) analysis

The nitrogen-physisorption (N_2-sorption) analysis was used to analyze surface characteristics, including surface area, pore volume, and pore diameter of porous materials. This technique explained by the adsorption/desorption of nitrogen gas at a temperature of -196°C, which provided the relationship between volume adsorbate (V_m) and relative pressure (P/P_0) called isotherm. Stephen Brunauer, Paul Hugh Emmett, and Edward Teller developed the BET model to measure the specific surface area (S_{BET}) of porous materials, which applied a multilayer adsorption system. The S_{BET} was calculated using the BET equation (Eq. 2.1). Besides, the amount of S_{BET} depended on the adsorbate molecule and adsorption mechanism [32].

$$\frac{P}{V(P_0-P)} = \frac{1}{CV_m} + \frac{C-1}{CV_m} - \frac{P_0}{P} \qquad (2.1)$$

Where:

V = volume adsorbate

P/P_0 = relative pressure

V_m = volume adsorbate at monolayer

C = BET constant

2.7.6 Fourier Transform Infrared spectroscopy (FTIR) analysis

Fourier Transform Infrared spectroscopy (FTIR) analysis was used to identify chemical bonds and surface functional groups of materials. The IR radiation was passed through the sample, some radiation was adsorbed, while some radiation was transmitted. The relationship between light adsorbed (%A) or transmitted (%T), and wave number called IR spectra, which corresponding to the frequency vibration of bonds in molecules. Thus, this technique can be specified the substance due to the difference in atoms and molecules of each material [33].

2.7.7 X-ray diffraction (XRD) analysis

The X-ray diffraction (XRD) analysis was used to identify the crystal structure and crystalline size of materials. The X-ray was generated from a cathode ray tube and passed through the sample. After that, the diffracted ray was collected the angle between the incident, then calculated the d-spacing using Bragg's law (Eq. 2.2). Therefore, this technique can be specified the crystalline material by comparing d-spacing with standard reference patterns. Furthermore, the crystalline size of materials can be calculated using the Debye-Scherrer's equation (Eq. 2.3) [34].

$$n\lambda = 2dsin\theta \quad (2.2)$$

Where:

n = diffraction order

λ = wavelength

d = lattice spacing

θ = diffraction angle

$$d = \frac{K\lambda}{Bcos\theta} \quad (2.3)$$

Where:

d = crystalline size

K = Scherrer constant

λ = wavelength

B = FWHM

θ = diffraction angle

2.7.8 NH_3 temperature Programed Desorption (TPD) analysis

Ammonia temperature-programmed desorption (NH_3-TPD) analysis was used to examine the acidity of the solid catalyst, such as alumina, zeolite, and activated carbon, etc. In this technique, the sample was exposed under the flow of ammonium, while the temperature was continuously increased. The number and strength of acid sites were determined by the correlation between desorbed ammonia and temperature (T). Typically, the NH_3-TPD performed under identical experimental conditions, which can be compared with other catalysts [35].

2.7.9 H_2 temperature Programed Reduction (TPR) analysis

Hydrogen temperature-programmed reduction (H_2-TPR) analysis was used to examine the reducibility of mixed metal oxide, metal oxide, metal sulfide, metal phosphide, and metal catalyst. In this technique, the sample was exposed under the flow of hydrogen, with the temperature increased. The oxidation state and reducibility were determined by the consumption of hydrogen at each temperature. Moreover, the H_2-TPR can be evaluated the optimum reducing temperature of the catalyst for study in various reactions [36].

2.7.10 Gas chromatography-mass spectroscopy (GC-MS) analysis

Gas chromatography-mass spectrometry (GC-MS) analysis was used to identify the substance, which combined two techniques. Gas chromatography (GC) was used to separate the component of mixtures, and mass spectroscopy (MS) was used to analyze each component. In the GC, mixtures in a mobile phase interacted with a stationary phase at different rates, which was separated into parts. The compound was eluted from the GC column, then entered to the MS and ionized into fragments. The mass of fragments divided by the charge called mass to charge ratio (M/Z). Therefore, the substance can be identified due to different M/Z, which was a fingerprint of each molecule.

2.8 Literature reviews

In this part, the relevant information of hydrodeoxygenation (HDO) of vegetable oil to clean diesel using a metal support catalyst was investigated. Furthermore, details about biofuel production, catalytic hydrodeoxygenation, and activated carbon (AC) preparation were summarized.

The continuously increased demand for fossil fuel and global warming caused by greenhouse gas (GHG) emission has prompted a worldwide search for alternative energy sources in the transportation section. Renewable energy resources, such as lignocellulosic materials, have bed of interest for many research teams for biofuel production. **Fig. 2.3** displays various methods of converting vegetable oil to clean diesel (i.e., green diesel and jet fuel), including pyrolysis, transesterification, and hydrodeoxygenation (HDO). Also, the HDO was the most considered method for biofuel production due to a shorter process, which provided the highest quality fuel.

Besides, the catalytic conversion of triglycerides entailed methods of hydrotreating, such as hydrogenation, hydrogenolysis, deoxygenation, decarboxylation, decarbonylation, hydrocracking, and isomerization. The summarized works by extensive research on the HDO of vegetable oil to produce clean diesel were collected in **Table 2.3**. Form the table, we found that feedstock, catalyst, and reaction conditions will directly affect the catalytic activity and fuel properties. Thus, the major challenge of the HDO process was the selection of feedstock, catalyst as well as reaction conditions [16]. The reviews on recent studies regrading this focus were summarized in all aspects.

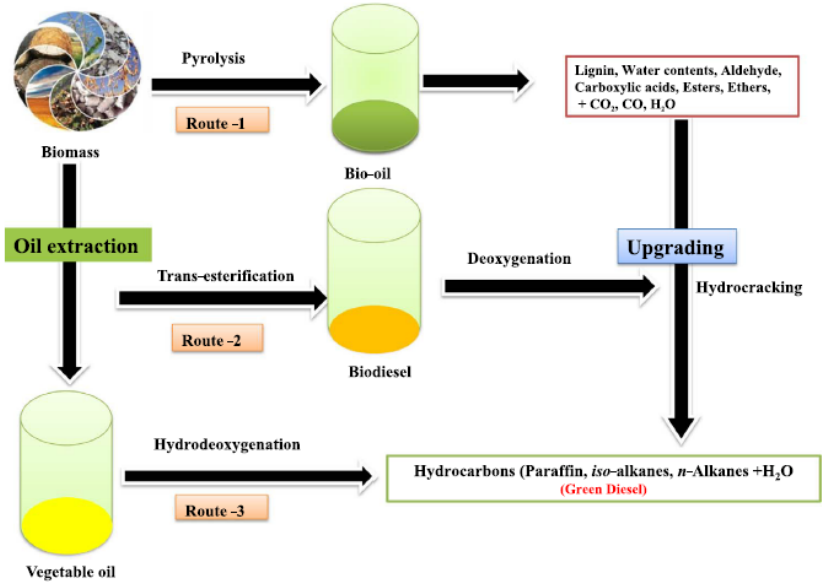

Figure 2.3 The conversion of vegetable oil to produce clean diesel [16]

Table 2.3 The HDO of vegetable oil to produce clean diesel [16]

Feed	Catalyst	P (bar)	T (K)	Time (h)	Reactor
Crude palm oil	$NiMo/Al_2O_3$	40-90	533-613	LHSV = 1 h^{-1}	trickle-bed
Vegetable oil and jatropha oil	1%Pt/HZSM5, Re/Al_2O_3	65, 85% H_2 in N_2	543-573	LHSV = 1-2 h^{-1}	fixed-bed
Rapeseed oil, refined and acidic vegetable oil	CoMo/MCM41, $NiMo/Al_2O_3$, $CoMo/Al_2O_3$	20-110, 33	573-593, 583.15-623.15	WHSV = 1-4 h^{-1}	fixed-bed
Soybean oil	$NiMo/Al_2O_3$, Ni/Si_2O-Al_2O_3, Pt/Al_2O_3, Pd/Al_2O_3, Ru/Al_2O_3	92	673	Catalyst/oil = 6.044	high pressure batch
Rapeseed oil	$NiMo/Al_2O_3$	70, 150	583.15-633.15	WHSV = 1 h^{-1}	laboratory flow
Rapeseed oil	CoMo/mesoporous Al_2O_3	7-70	523-623	WHSV = 1.5 h^{-1}	fixed-bed
Rapeseed oil	Ni/Al_2O_3, Mo/Al_2O_3, $CoMo/Al_2O_3$	35	583	WHSV = 2 h^{-1}	fixed-bed
Oleic acid and canola oil	Mo/Al_2O_3, W/Al_2O_3, V/Al_2O_3	715	653-683	LHSV = 0.45 h^{-1}	quartz tubular
Vegetable oil	$NiMo/SiO_2$-Al_2O_3	H_2/oil = 800 ml/ml	623	LHSV = 7.6 h^{-1}	fixed-bed
Rapeseed oil	Pt/HZSM5, $NiMo/Al_2O_3$	50-110	573-673	LHSV = 3 h^{-1}	batch

Sunflower oil	Commercial hydrocracking	180	633-693	WHSV = 1.5 h^{-1}	fixed-bed
Waste cooking oil	Commercial hydrocracking	827-965	603-671	LHSV = 0.5-1 h^{-1}	small-scale pilot plant unit

It is well known that the catalyst played a vital role in triglycerides conversion, which affected product properties. The most excellent catalyst in the HDO process was noble metal (e.g., Pd, Pt, Ru, and Rh) supported on silica, alumina, and activated carbon (AC). Al-Muhtaseb A.a.H. et al. [4] studied the production of second-generation biofuel, including green diesel and jet fuel, via the HDO of date pit oil using Pd/C and Pt/C catalyst. The powdered date pit was carbonized at 500°C for 5 h under the N_2 atmosphere to produce AC. After that, the AC was impregnated with 4 wt% of palladium and platinum chloride to produce Pd/C and Pt/C catalyst, respectively. The biofuel was provided through the HDO of date pit oil in the Parr reactor at 300°C for 5 h with 1 MPa of H_2 pressure. The results indicated that synthesized catalysts were highly active in the HDO process due to well-dispersed of Pd and Pt nanoparticles on the AC support, as showed in **Fig. 2.4** and **Table 2.4**. The liquid hydrocarbons formed within the range of 72.1 and 72.9% green diesel, and 30.4 and 28.4% jet fuel using Pd/C and Pt/C catalyst, respectively (**Table 2.5**). It can be concluded that the waste date pit was a promising platform for the production of AC and high-quality fuel.

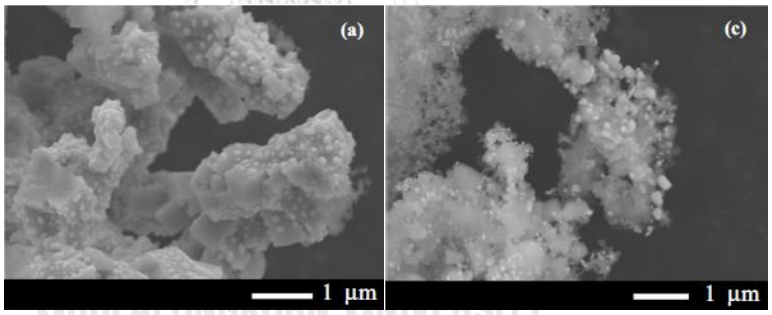

Figure 2.4 SEM images of (a) Pb/C and (c) Pt/C catalyst [4]

Table 2.4 Specific surface area, pore volume, pore diameter, and metal dispersion of Pd/C and Pt/C catalyst [4]

Properties	C	Pt/C	Pd/C
S_{BET} (m^2/g)	432.1	297.3	304.3
Pore volume (cm^3/g)	0.22	0.13	0.19
Pore diameter (Å)	7.62	6.56	7.34
Metal dispersion (%)	-	81	87

Table 2.5 Detailed composition of paraffin hydrocarbons obtained from the HDO of date pit oil [4]

Components	Pd/C	Pt/C
Decane	1.23	1.07
Undecane	3.21	3.81
Dodecane	14.2	12.9
Tridecane	2.16	2.27
Tetradecane	7.19	7.07
Pentadecane	2.42	1.12
Hexadecane	6.11	6.94
Heptadecane	14.1	14.3
Octadecane	49.4	50.4

Besides, de Sousa F.P. et al. [13] studied the production of clean diesel, including gasoline, jet fuel, and green diesel, via the HDO of palm kernel oil using Pd/C catalyst. In this study, the reaction was processed in the Parr reactor to ensure the catalytic activity. The palm oil was added to the reactor and heated up to 300°C for 5 h with 1 MPa of H_2 pressure. The liquid hydrocarbons obtained from the HDO process consisted of $C_{9\text{-}17}$, which C_{11} was a predominant product, as showed in **Fig. 2.5**. In addition, the decarboxylation and decarbonylation reactions were favored in this study, indicated the presence of odd chain hydrocarbon in products. The palm kernel oil was great potential for the production of jet fuel, which oil conversion of 96% and jet fuel selectivity of 82%, as showed in **Fig. 2.6**. Moreover, 5% of deoxygenation products mixed with commercial jet fuel can be employed in commercial aircraft without any modification.

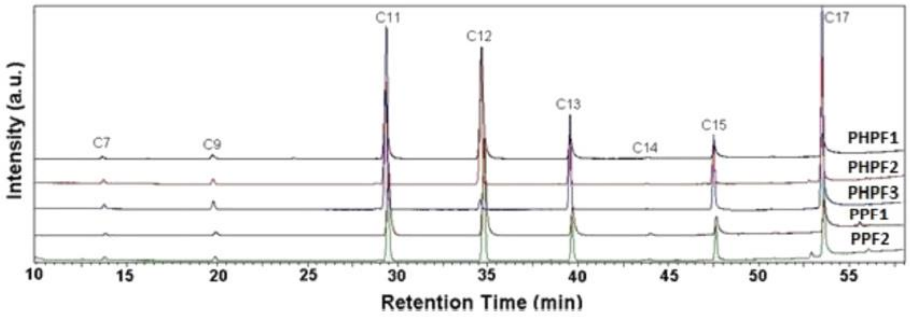

Figure 2.5 Chromatograms of liquid hydrocarbon products obtained from the HDO of palm kernel oil [13]

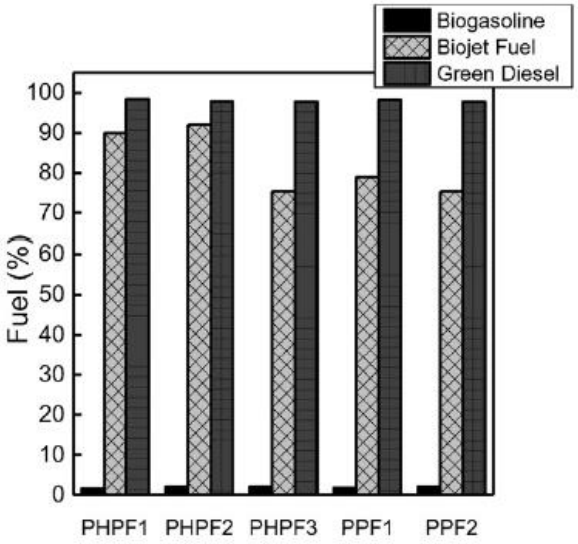

Figure 2.6 Theoretical percentages of biofuel obtained from the distillate of liquid hydrocarbon products [13]

However, the use of noble metal catalysts still limited due to the relatively high catalyst precursor price. Therefore, the development of transition metal catalyst (e.g., Fe, Co, Ni, Cu, Mo, and W, etc.) has been interested in many researches. Also, the transition metal phosphide has been described as a family of high activity hydrotreatment catalyst owing to their low cost, abundance, and high efficiency. Shi, H., et al. [37] investigated the use of Ni-based phosphide catalyst supported on SiO_2, Al_2O_3, TiO_2, SAPO-11, HY, and CeO_2 for the deoxygenation of methyl laurate. The support was incipiently impregnated with 15 wt% of nickel nitrate and diammonium hydrogen phosphate with the ratio of 1:1 (Ni:P) to produce NiP catalysts. The HDO of methyl laurate was tested on a stainless-steel fixed bed reactor at 573-613 K with 2 MPa

of H_2 pressure. The conversion of methyl laurate and C_{11-12} selectivity tended to decrease in the sequence of NiP/SiO_2 > NiP/Al_2O_3 > NiP/TiO_2 > NiP/SAPO-11 > NiP/HY > NiP/CeO_2. As showed in **Fig. 2.7**, the NiP/SiO_2 catalyst was the highest methyl laurate conversion and C_{11-12} selectivity due to the high surface area and acidity, which affected deoxygenation and hydrocracking reaction. This study proposed that catalytic activity was correlated with the characteristic of catalysts, especially surface and acidity property.

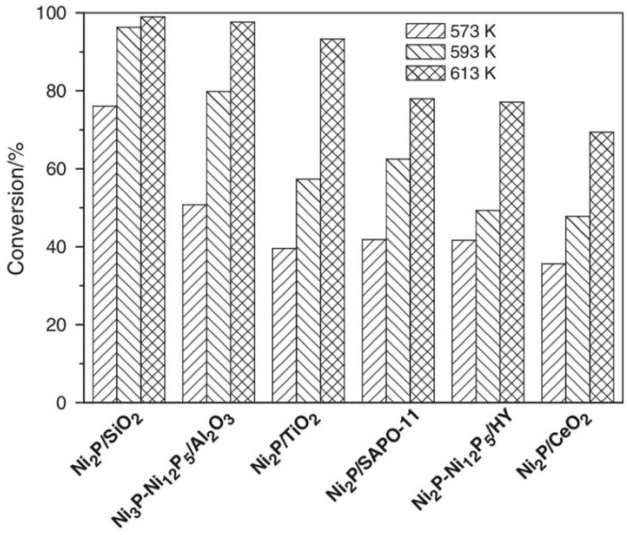

Figure 2.7 Deoxygenation of methyl laurate on NiP-based catalysts [37]

Alvarez-Galvan, M.C., et al. [38] reported the preparation of silica-supported Ni, Co, Fe, Mo, and W phosphide catalyst. The 15 wt% of metal phosphide supported silica catalysts were prepared by the incipient wetness impregnation, followed by the reduction method. As-prepared catalysts were tested the HDO of methyl laurate on a trickle-bed reactor at 553-573 K, 1-3 MPa, liquid flow 0.2-0.4 ml/min, and H_2/liquid ratio of 300. The XRD patterns of reduced catalysts showed in **Fig. 2.8**, the diffraction line of the MoP catalyst was not observed, indicating a well-dispersed MoP on the SiO_2 surface. Besides, the NH_3-TPD profiles of MoP catalyst **(Fig. 2.9**) presented mostly weak and medium acid sites, which related to the overlap contribution of Brønsted (P-OH) and Lewis (M^{d+}) acid sites. The activity of as-prepared catalysts showed in **Table 2.6**, the conversion of methyl laurate tended to decrease in the sequence of MoP > CoP > NiP > WP ≈ FeP. The results revealed the MoP catalyst exhibited the best catalytic

performance due to a higher active phase dispersion and its moderate acidity, which promoted the deoxygenation as well as hydrocracking reaction.

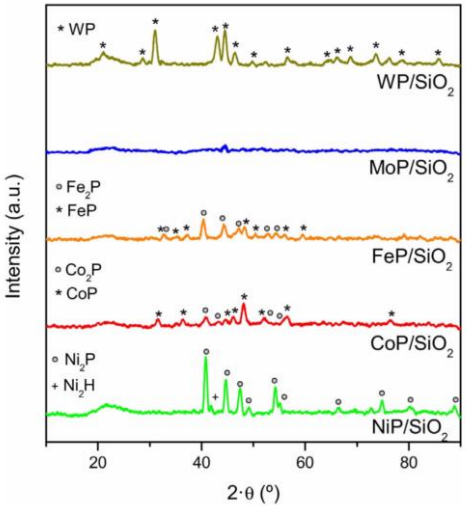

Figure 2.8 XRD patterns of reduced catalysts [38]

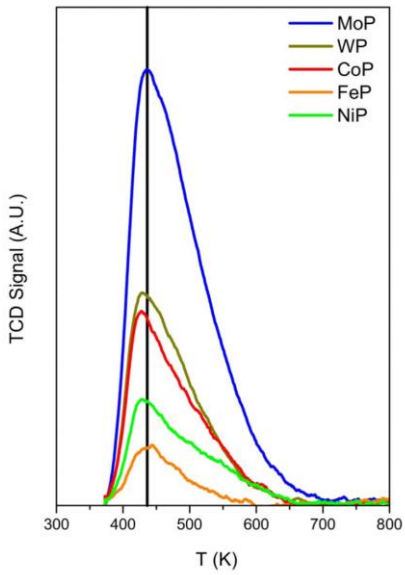

Figure 2.9 NH_3-TPD profiles of reduced catalysts [38]

Table 2.6 Catalytic activity results at steady state of reduced catalysts [38]

Catalyst	Methyl laurate conversion (%)	HC C_{12} (%)	HC C_{11} (%)	HC C_{6-10} (%)	Others (%)
NiP/Si_2O_3	71.9	17.3	72.3	8.7	0.8
CoP/Si_2O_3	77.6	12.4	76.3	9.8	0.5
FeP/Si_2O_3	18.6	9.0	27.3	-	17.2
MoP/Si_2O_3	86.0	94.5	4.2	0.8	0.5
WP/Si_2O_3	22.5	25.5	4.4	-	16.5

Generally, the catalyst support plays an essential role in active phase dispersion and catalytic performance. The uniform distribution of the metal catalyst on the support will enhance the catalytic activity and protect catalyst deactivation. Several materials, such as silica, alumina, zeolite, and activated carbon (AC), were widely used as catalyst support in the hydrotreating process. Furthermore, the AC was considered as an interest material for used as catalyst support owing to cost-effective and environmentally friendly materials.

The AC derived from agriculture waste or petroleum residue was utilized as catalyst support in various researches. Therefore, the synthesized parameters, such as temperature, time, and activation methods, will directly influence the resultant AC properties. There were many research studies focused on the preparation of AC from agriculture waste and petroleum residue.

Basically, the production of AC from agriculture waste and petroleum residue consisted of a two-steps process, namely the carbonization and activation process. The carbonization process was an endothermic reaction, which operated at a temperature range of 300-900°C to produce carbon materials. The surface properties of such materials were enhanced by the activation process, including physical and chemical activation. The physical activation, used an oxidant gas (e.g., steam, CO_2, and ozone, etc.) to activate carbon materials at a temperature above 600°C. While, the chemical activation, used a chemical reagent (e.g., H_3PO_4, NaOH, KOH, and $ZnCl_2$, etc.) to activate carbon materials at low temperature. The produced AC has a high surface area and large pore volume, which suitable for used as catalyst support. Besides, the

chemical activation was more preferred than the physical activation due to the shorter time, higher yield, and higher microporosity. Additionally, many studies claimed that KOH was the best activating agent in AC production, which provided a high surface area with large microporosity of AC.

Hui, T.S. et al. [39] collected research works, which related to the preparation of AC from various carbonaceous materials by KOH activation, as showed in **Table 2.7**. The results revealed that an activating agent ratio (KOH:C) will directly affect the surface characteristics of AC. Besides, the produced ACs have a high surface area and large microporosity (~90%). This study also confirmed that activation with alkali hydroxide will enhance the surface properties of AC

Table 2.7 Preparation of activated carbon by KOH activation [39]

Raw material	Carbon content (%)	Impregnation ratio (KOH:C)	Activation procedure	Yield (%)	Surface area (m^2/g)	Microporosity (%)
Palm kernel shell	23	1:1	Carbonization, N_2, 400°C, 1 h, activation, N_2, 800°C, 15 min	46.3	20	68.8
Palm kernel shell	23	1:1	Carbonization, N_2, 400°C, 1 h, activation, N_2, 800°C, 45 min	-	127	91.7
Corn cob	46.5	3:1	Carbonization, N_2, 400°C, 1 h, activation, N_2, 800°C, 120 min	-	1600	-
Rice husk	27	5:1	Carbonization, N_2, 400°C, 4 h, activation, N_2, 850°C, 60 min	17.5	1499	36.2
Sewage sludge	68.7	-	Carbonization, N_2, 400°C, 2 h, activation, N_2, 800°C, 30 min	-	920	61
Grape seed	48.7	1:1	Activation, N_2, 600°C, 60 min	35.7	784	93.7
Peanut shell	45.3	1:1	Activation, N_2, 450°C, 60 min	-	88.9	24.2
Textile sewage sludge	-	1:1	Activation, N_2, 500°C, 60 min	-	135	-
Sewage sludge	48.7	3:1	Activation, N_2, 750°C, 30 min	-	1832	67.6

Walnut shell	21.4	2:1	Carbonization, N_2, 700°C, 60 min, activation, N_2, 600°C, 60 min	23.4	657	85.4
Kraft lignin	56.5	3:1	Activation, N_2, 550°C, 2 h	41	959	69.4
Bamboo waste	45.5	2:1	Activation, N_2, 800°C, 3 h	-	1533	-

Huang, Y. et al. [40] studied the production of AC from the wood-based fiber. The fiber precursor was carbonized at 500°C for 1 h under the N_2 atmosphere, then soaked in KOH solution of 20%. After that, KOH-impregnated fiber was activated at 850°C for 1 h under the N_2 atmosphere to obtain the AC. The physicochemical properties, such as morphology, carbon content, and surface properties of AC, were also investigated. The combination of carbonization and KOH activation resulted in the development of AC's surface properties, which provided high surface area and large microporosity.

Gao, Y. et al. [41] studied the preparation of AC from the lignin of black papermaking liquor. The lignin precursor was mixed with KOH at a ratio of 0.5-4, then activated at 650-850°C for 0.5-2.5 h under the N_2 atmosphere. The effect of the lignin/KOH ratio, activation temperature, and activation time on the BET surface area was investigated. The results revealed that the lignin/KOH ratio was the main factor influencing the surface properties of AC. The BET surface area continuously increased with the lignin/KOH ratio increase and reached a maximum at the ratio of 3:1. Besides, above this ratio, the BET surface area decreased due to the pore widening by KOH activation. The maximum surface area (2943 m^2/g) was obtained at lignin/KOH ratio of 3:1, activation temperature of 750°C, and activation time of 1 h.

Sayed Ahmed, S.A. et al. [42] investigated the production of AC from petroleum coke, a by-product of the petrochemical industry. Petroleum coke precursor was mixed KOH with a ratio of 1, 2, and 4, then carbonized at different temperatures and times. The textural properties of AC were determined by the adsorption of N_2 at -196°C. From this study, they found that a ratio of KOH/Coke was the most critical factor affecting surface characteristics of AC. The surface area and non-micropore volume increased, whereas the micropore volume decreased with a ratio of KOH/Coke increase. Thus, the increase in the surface area resulted from pore formation by the evolution of gases products and metal salt during the activation.

Mohammadi, S. et al. [43] studied the preparation of AC from oil sludge, which contained 80 wt% aliphatic hydrocarbons. The oily sludge was physically mixed with KOH in a ratio of 2:1, then carbonized at 600°C for 1 h under the N_2 atmosphere. The

surface area and porosity of produced AC were measured by N_2 adsorption/desorption at -196°C. The BET surface area, total pore volume, and micropore surface area of AC was 328.0 m^2/g, 0.21 cm^3/g, and 289.1 m^2/g, respectively. The results suggested the thermochemical treatment of oily sludge can be produced AC with a developed pore structure. Thus, this study showed the feasibility of industrials waste derived AC, which considered as valuable materials.

As described above, the development of AC's surface properties will affect catalytic activity and biofuel properties. There were many research works focused on the production of AC from agricultural waste. In contrast, this study used industrial waste, such as slop oil for the production of AC. Furthermore, the study of synthesis of AC, preparation of MoP catalyst supported on AC, and HDO reaction were investigated.

CHAPTER 3
RESEARCH METHODOLOGY

In this study, the experimental works were divided into three steps (**Fig. 3.1**). First, the synthesis and characterization of activated carbon (AC) from heavy fuel oil (HFO) were examined. Secondly, the preparation and characterization of molybdenum phosphide (MoP) catalyst impregnated on AC were further investigated. Finally, catalytic testing in hydrodeoxygenation (HDO) of vegetable oil was conducted to confirm the performance of the MoP catalyst impregnated on AC. The details of experimental methodologies and characterization techniques were described in this chapter.

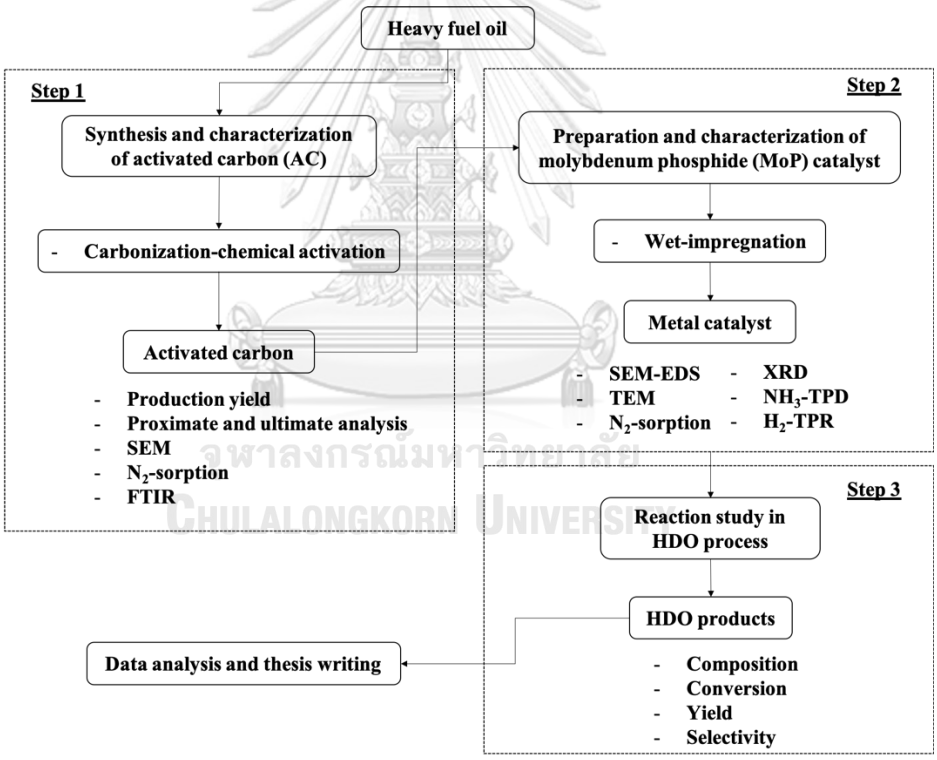

Figure 3.1 Methodology of this study

3.1 Materials and chemicals

Heavy fuel oil (HFO) from PTT and Retail Business Public Company Limited and Sulfuric acid (H_2SO_4) (96%) from CARLO ERBA Reagents was used as carbon precursor and oxidizing agent, respectively. Nitrogen gas (N_2) (99.99%) from Praxair

Thailand and Potassium hydroxide (KOH) (≥ 85%) from CARLO ERBA Reagents was employed as a blankting gas and activating agent, respectively. Ammonium molybdate tetrahydrate $(NH_4)_6Mo_7O_{24}\bullet 4H_2O$ (≥ 99%) and di-Ammonium hydrogen phosphate $(NH_4)_2HPO_4$ (≥ 99%) from CARLO ERBA Reagents was used as molybdenum and phosphorus precursor. Vegetable oil from Morakot Industries Public Company Limited and Hydrogen gas (H_2) (99.99%) from Praxair Thailand was utilized as raw materials for HDO reaction. All chemicals were used as received.

3.2 Synthesis and characterization of activated carbon

HFO was used as raw material, and sulfuric acid (H_2SO_4) was used as an oxidizing agent. The one-step process (carbonization-chemical activation) was chosen for the synthesis of AC. **Fig. 3.2** shows a schematic diagram of the experimental apparatus. A quartz tube reactor with 2 mm O.D. and 1200 mm length were divided into three heating zones (namely T1, T2, and T3) using a set of temperature and mass flow controllers.

Firstly, HFO was mixed with sulfuric acid (H_2SO_4) with a ratio of 4:1 (H_2SO_4:HFO) at 100°C for 1 h to become a solid carbon-rich substance. After that, the solid product was washed with deionization (DI) water until neutral pH and dried overnight. Secondary, the solid product was mixed continuously with potassium hydroxide (KOH) with a ratio of 0.5, 1, 1.5, and 2 :1 (KOH:HFO) and then subjected to a heating zone (T2). Thirdly, then quartz tube reactor was heated from ambient to desired temperature (400, 500, 600, and 700°C), with heating rate 10°C/min under N_2 atmosphere and hold for 1 h to enhance carbon percentage then, the resulting AC was cooled down to room temperature. After that, the AC product was washed with DI water until neutral pH and dried thoroughly. Every sample was denoted as AC-XXX-Y:Y, where XXX is carbonization temperature (400-700°C), and Y:Y is ratio of KOH to C (0.5-2:1). For example, AC-700-1:1 refers to AC prepared at 700°C with a KOH to C ratio of 1:1.

The production yield of AC was calculated based on its gravimetric measurement (Eq. 3.1), considered the mass of produced AC (m_f) to the mass of HFO feedstock (m_0).

$$Yield\ of\ AC\ (\%) = \frac{m_f}{m_0}\ x\ 100 \qquad (3.1)$$

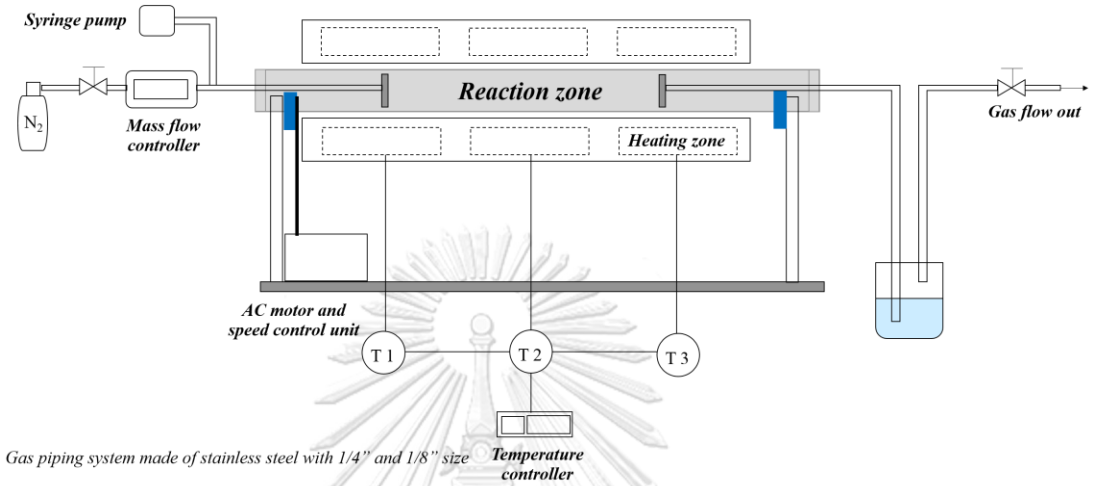

Figure 3.2 Schematic diagram of quartz horizontal tube reactor

As-prepared AC was characterized by proximate and ultimate analysis, Scanning electron microscopic (SEM) analysis, N_2 adsorption-desorption (N_2-sorption) analysis, and Fourier transform infrared spectroscopic (FTIR) analysis. The details of the characterization techniques were described as follows,

3.2.1 Proximate and ultimate analysis

Proximate analysis was completed using a Thermogravimetric analyzer (TGA, PerkinElmer Pyris 1, USA). This technique demonstrated four compositions of AC, including moisture, volatile matter, ash, and fixed carbon. Typically, as-prepared AC was heated from 30 to 900°C with a heating rate of 10°C/min under N_2 flow. The moisture, volatile matter, and ash contents were measured according to the ASTM D2867-99, ASTM D5832-98, and ASTM D2866-94 standard methods, respectively [44]. Whereas, fixed carbon content was calculated by subtracting from the other compositions.

Ultimate analysis was determined using a CHN elemental analyzer (CHN, Leco truspec chn-628, UK). This technique illustrated elemental compositions of AC in terms

of carbon (C), hydrogen (H), and nitrogen (N). The oxygen (O) composition was directly calculated by the difference of all arrangements from 100% [45].

3.2.2 Scanning electron microscopic (SEM) analysis

Surface morphology of as-prepared AC was observed using a Scanning Electron Microscope (SEM, Zeiss EVO50, Germany) operated at 10 eV. Before the analysis, the sample was sputtered with gold to enhance its surface conductivity.

3.2.3 N_2 adsorption-desorption (N_2-sorption) analysis

Surface property and pore structure of as-prepared AC were determined from the adsorption-desorption isotherm of nitrogen operated at -196°C, using a gas sorption analyzer (Quantachrome Autosorp iQ-MP-XR, Germany). The specific surface area (S_{BET}) was carried out by using the Brunauer-Emmett-Teller (BET) model. Pore size distributions were analyzed by using the Density Functional Theory (DFT) model. The total pore volume (V_T) was measured by condensation of liquid nitrogen at a relative pressure of 0.99, while the micropore volume was evaluated by using the T-plot model.

3.2.4 Fourier-transform infrared spectroscopic (FTIR) analysis

Surface functional groups of as-prepared AC were analyzed using Fourier-Transform Infrared Spectroscopy (FTIR, PerkinElmer UATR Two, UAS). The IR spectra were acquired in the range of 400-4000 cm^{-1}, with a resolution of 4 cm^{-1}. The solid specimens were prepared by a conventional method and used air as a background of the experiment [46].

3.3 Preparation and characterization of molybdenum phosphide catalyst impregnated on AC

As-prepared AC was crushed and sieved in a range of 1.5-5 mm. Then, MoP loaded into AC was prepared by the wet-impregnation technique using ammonium molybdate tetrahydrate $(NH_4)_6Mo_7O_{24} \bullet 4H_2O$ and di-Ammonium hydrogen phosphate $(NH_4)_2HPO_4$ as molybdenum and phosphorus precursor, respectively with various metal phosphide loading of 5, 10, 15, and 20 wt%. Firstly, ammonium molybdate and di-Ammonium hydrogen phosphate were mixed with a ratio of 1:1 ($(NH_4)_6Mo_7O_{24} \bullet 4H_2O$: $(NH_4)_2HPO_4$), then a fixed amount of AC was added into an aqueous solution.

Then, the suspension was continuously mixed at 60°C for 3 h. The catalyst was dried at 105°C overnight, then calcined at 700°C for 2 h under N_2 atmosphere to remove impurities. After that, the catalyst was reduced at 600°C for 3 h under H_2 atmosphere to obtain the corresponding metal-phosphide form. Furthermore, the catalyst was denoted as 5MoP-AC, 10MoP-AC, 15MoP-AC, and 20MoP-AC, which represents an amount of metal phosphide loading.

The MoP-AC catalyst was characterized using various techniques, which were Scanning electron microscopic-Energy dispersive spectrometry (SEM-EDS) analysis, Transmission electron microscopic (TEM) analysis, N_2 adsorption-desorption (N_2-sorption) analysis, X-ray diffraction (XRD) analysis, Ammonia temperature-programmed desorption (NH_3-TPD) analysis and Hydrogen temperature-programmed reduction (H_2-TPR) analysis to explore the properties of the catalyst for HDO of vegetable oil, which was described in detail as follows,

3.3.1 Scanning electron mxicroscopic-Energy dispersive spectrometry (SEM-EDS) analysis

Surface morphology and elemental composition of the MoP-AC catalyst were obtained using a Scanning Electron Microscope equipped with an Energy Dispersive X-ray Spectrometry (SEM-EDS, Zeiss EVO50, Germany) operated at 10 eV. The sample was coated by gold sputtering to enhances its conductivity before analysis.

3.3.2 Transmission electron microscopic (TEM) analysis

Surface morphology and particle size distributions of the MoP-AC catalyst were performed using a Transmission Electron Microscope (TEM, TEM JEOL-JEM-2100plus, Japan) operated at 200 eV. Before measurement, the sample was dropped onto a Cu grid from ethanol suspension.

3.3.3 N_2 adsorption/desorption (N_2-sorption) analysis

Surface characteristics of the MoP-AC catalyst were determined from the adsorption-desorption isotherm of nitrogen operated at -196°C, using a gas sorption analyzer (Quantachrome Autosorp iQ-MP-XR, Germany). The specific surface area (S_{BET}), pore size distributions (V_T), total pore volume (V_T), and micropore volume (V_{mi})

were analyzed by using the BET, DFT, condensation of liquid nitrogen at a relative pressure of 0.99, and T-plot method, respectively.

3.3.4 X-ray diffraction (XRD) analysis

The crystal structure and crystalline size of the MoP-AC catalyst were determined using an X-ray diffractometer (XRD, SmartLab, Rigaku, Japan), with a Cu-Kα radiation (λ = 0.154 nm). The diffraction patterns were recorded over a range of Bragg angles (2θ) between 10 and 80°, with a scanning rate of 0.02°/step. The mean crystalline size was determined using the Debye-Scherrer's equation.

3.3.5 NH_3 temperature-programmed desorption (NH_3-TPD) analysis

Acidity property of the MoP-AC catalyst was measured by an Ammonia temperature-programmed desorption (NH_3-TPD) technique, using a Quantachorm Chemisorption analyzer (ChemStar TPX, Germany). The sample was reduced with a H_2 flow at 650°C for 1 h. After the reduction, 5% of NH_3 mixed with He was passed through the sample at 100°C for 30 min. Next, the sample was swept with He flow at 100°C for 30 min to remove an adsorbed NH_3. Afterward, NH_3-TPD was performed in a He flow from 100°C to 800°C with a heating rate of 10°C/min. The desorbed NH_3 was detected by the thermal conductivity detector (TCD).

3.3.6 H_2 temperature-programmed reduction (H_2-TPR) analysis

Reducibility property of the MoP-AC catalyst was analyzed by a Hydrogen temperature-programmed reduction (H_2-TPR) technique, using a Quantachorm Chemisorption analyzer (ChemStar TPX, Germany). The sample was purged with a He flow at 120°C for 1 to remove moistures and volatile gases. The H_2-TPR was elevated in the flow of 5% H_2 balanced with Ar from 100 to 800°C with a heating rate of 10°C/min. The H_2 consumption was monitored by the thermal conductivity detector (TCD).

3.4 Reaction study in HDO process

In this work, a custom-made continuous-flow trickle-bed reactor was employed to test the performance of MoP impregnated on AC. The experimental apparatus reactor (**Fig. 3.3**) was made from stainless steel 316 with 7 mm diameter and 700 mm length.

The reactor system consisted of three sub-units, including feed unit, reaction test unit, and collection unit. The temperature was controlled by the K-type temperature controller in an electrical tube furnace, while the back-pressure regulator controlled the pressure. The HPLC pump controlled the feed flow rate, and the mass flow controller also managed the gas flow rate. Moreover, the as-prepared catalyst was placed in the middle of the reactor for uniform temperature distribution and reduced pressure drop.

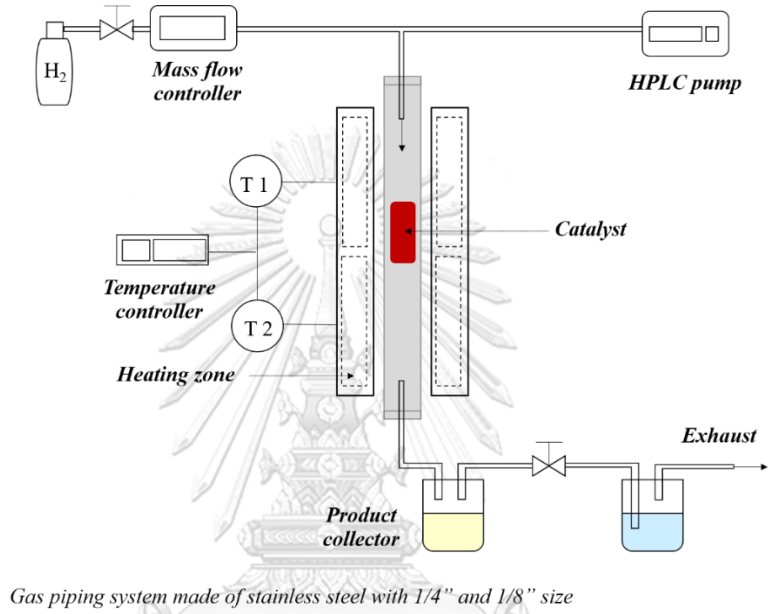

Figure 3.3 Schematic diagram of continuous-flow trickle-bed reactor

The activity of the MoP-AC catalysts was evaluated for HDO of vegetable oil to produce clean fuel. The reduced MoP-AC catalyst was placed in the reactor as temperature increased from ambient to desired temperature (400, 420, and 440°C) (10°C/min) then pressurized with H_2 (150 cc/min) to 50 bar. Vegetable oil feedstock obtained was pumped to the reactor with liquid hourly space velocity (LSHV) = 1 h^{-1} (0.134 cc/min), H_2/oil ratio was kept at 1000 N cm^3/cm^3 and maintained for 2 h. The liquid product was collected, and separated water phase then kept for further analysis. Moreover, the long-term stability of the optimum catalyst was tested to investigate the catalyst deactivation. The reactor was operated using the same conditions, which reaction temperature of 420°C and maintained continuously for 24 h.

The oil product was analyzed using a Gas Chromatography equipped with a Mass spectrometer and a capillary column (DB-1HT, 30 m x 0.32 mm x 0.1 μm) (GCMS, GCMS-QP2020, Shimadzu, Japan) [4]. The peaks were identified using the GCMS solution software with a database to determine the product composition. The oil conversion and liquid HC yield were determined based on the mass balance of the initial amount of feed oil (m_0) and the final amount of oil (m_f). The selectivity of green diesel and bio jet-oil were calculated, using the following equations:

$$Oil\ conversion\ (\%) = \frac{m_0 - m_f}{m_0} x\ 100 \quad (3.2)$$

$$Liquid\ HC\ yield\ (\%) = \frac{m_f}{m_0}\ x\ 100 \quad (3.3)$$

$$Green\ diesel\ selectivity\ (\%) = \frac{m_{green\ diesel}}{m_{oil\ converted}} x\ 100 \quad (3.4)$$

$$Bio\ jet\text{-}oil\ selectivity\ (\%) = \frac{m_{bio\ jet-oil}}{m_{oil\ converted}} x\ 100 \quad (3.5)$$

Furthermore, bio jet-oil compositions in terms of C number ($C_{9\text{-}14}$) and HC structure (e.g. n-paraffin, iso-paraffin, cyclo-paraffin, olefin and aromatic) was examined. The %contribution of HDO and DCO/DCO_2 was also investigated, using the following equations:

$$HDO\ (\%) = \frac{m_{even\ number}}{m_{oil\ converted}} x\ 100 \quad (3.6)$$

$$DCO/DCO_2\ (\%) = \frac{m_{odd\ number}}{m_{oil\ converted}} x\ 100 \quad (3.7)$$

CHAPTER 4
RESULTS AND DISCUSSION

4.1 Synthesis of activated carbon

The activated carbon (AC) was synthesized from heavy fuel oil (HFO) via the one-step process (carbonization-chemical activation). The properties of as-prepared AC, which was essential for application as catalyst support (i.e., production yield, proximate and ultimate analysis, surface morphology, surface properties, and surface functional group), were analyzed. The effect of the carbonization temperature and activating agent ratio on AC properties were also investigated to determine the optimum condition of AC support.

4.1.1 Effect of carbonization temperature

Fig. 4.1 demonstrates the production yield of carbonized products obtained from the carbonization of HFO with different temperatures. The production yield of carbonized products was approximately 21.9%. The production yield decreased with the increase in the carbonization temperature due to the thermal decomposition of organic substances, which was the loss of volatile matter and moisture contents. The disappearance of such substances revealed carbon formation, which was the most durable structure. The results confirmed that the carbonized products mainly consisted of carbon.

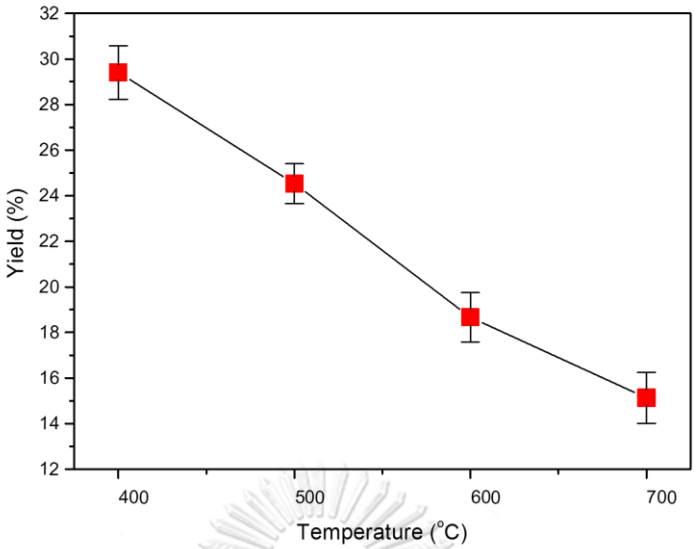

Figure 4.1 Production yield of carbonized products

The proximate analysis of carbonized products, including moisture, volatile matter, fixed carbon, and ash represented in **Table 4.1**. The volatile matter content decreased with the increase in the carbonization temperature due to the volatile decomposition during the carbonization process. In contrast, the fixed carbon and ash content increased with the elevated carbonization temperature. The fixed carbon content of carbonized products was in the range of 59.6-83.8%. However, the slightly increased moisture content resulted from gas and liquid absorption ability due to the increase in the porosity of carbon materials. The ultimate analysis of carbonized products, including C, H, N, and O showed in **Table. 4.1**. The C content increased with the increase in the carbonization temperature, while the H, N, and O content decreased due to the complete oxidation of H and O atoms during the carbonization process. The carbonized products contained high C content of 75.6-86.6%, which was similar to conventional carbon materials. In addition, the small amount of N content resulted from the nature of raw materials and moisture adsorbed during the measurement.

Table 4.1 Proximate and ultimate analysis of carbonized products

Sample	Moisture (wt%)	Volatile (wt%)	Fixed carbon (wt%)	Ash (wt%)	C (wt%)	H (wt%)	N (wt%)	O (wt%)
HFO	10.2	57.2	31.7	0.9	64.9	7.8	9.2	18.1
C-400	1.7	35.1	59.6	3.6	75.6	6.7	0.5	17.2
C-500	2.0	27.5	66.6	3.9	82.0	3.9	0.5	13.6
C-600	3.1	8.6	83.7	4.6	82.3	5.1	0.3	12.3
C-700	3.4	8.1	83.8	4.7	86.8	1.9	0.7	10.6

The surface morphology of the blank sample (HFO) and carbonized products was characterized by using a scanning electron microscope. **Fig. 4.2** displays the morphology of blank HFO and carbonized products obtained at a temperature of 400, 500, 600, and 700°C. As showed in **Fig. 4.2a** the blank sample displayed a non-porous agglomeration of carbon materials. **Fig. 4.2b-e** exhibited complicate porous structure, which rougher and irregular surfaces resulted from the thermal degradation of organic substances. Moreover, the carbonization temperature increase led to the rise in porous structure collapse. At a low carbonization temperature (400-600°C), the porous structure was not fully developed, while the temperature up to 700°C, a well-developed porous structure was observed. Thus, the optimum carbonization temperature was 700°C, which provided high porous structures of carbon materials.

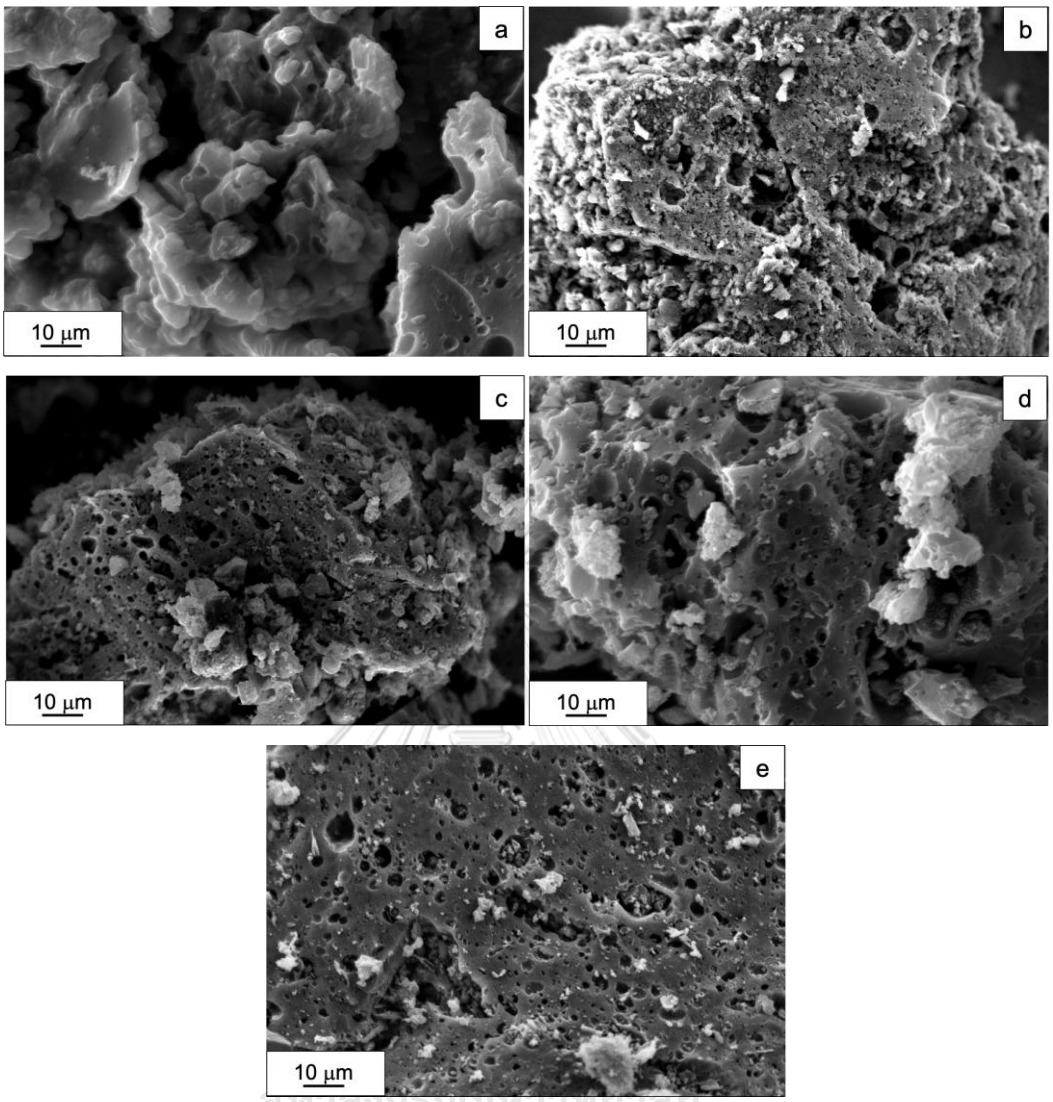

Figure 4.2 SEM micrographs of (a) HFO, carbonized product (b) C-400, (c) C-500, (d) C-600 and (e) C-700°C

The surface properties of carbonized products were analyzed by using the N_2-physisorption technique. **Table. 4.2** shows the BET surface area (S_{BET}), total pore volume (V_T), micropore volume (V_{mi}), and average pore diameter (D_{avg}) of carbonized products obtained from the carbonization with different temperatures. The surface area and pore volume were increased from 9.4 m^2/g and 0.026 cm^3/g to 48.6 m^2/g and 0.051 cm^3/g with the carbonization temperature was increased from 400 to 700°C, respectively due to the development of porous structure by the thermal treatment process. It was corresponding to the results of SEM images, which showed the increase in porous structure as the temperature increased. It could be observed a few pore

structures with a large diameter of 4.2-15.2 nm. However, the surface properties of carbonized products were not adequately used as catalyst support. Therefore, the activation process was required to improve the surface properties to provide a high surface area and large pore volume of AC.

Table 4.2 Surface properties of carbonized products

Sample	S_{BET} (m^2/g)	V_T (cm^3/g)	V_{mi} (cm^3/g)	D_{avg} (nm)
C-400	9.4	0.026	0.000	15.2
C-500	26.5	0.041	0.002	7.8
C-600	30.5	0.048	0.002	7.0
C-700	48.6	0.051	0.003	4.2

From this study, the optimum carbonization temperature was 700°C, which provided a uniform porous structure with high carbon content (86.6%) and large surface area (48.6 m^2/g). In this study, the activation temperature was fixed at 700°C, and the effect of the activating agent ratio was investigated, which was continually described.

4.1.2 Effect of activating agent ratio

The production yield of AC products obtained from the carbonization-chemical activation process with different activating agent ratio was also examined. As showed in **Fig. 4.3,** the production yield of AC products slightly decreased with the increase in the KOH ratio. The results suggested that the amount of KOH would not be affected the yield of AC. The slight decrease in the production yield was resulted from the loss of volatile matter and moisture contents, which were vaporized during the activation process. As mentioned above, it can be concluded the carbonization temperature was the most critical factor that affected the yield of resultant products.

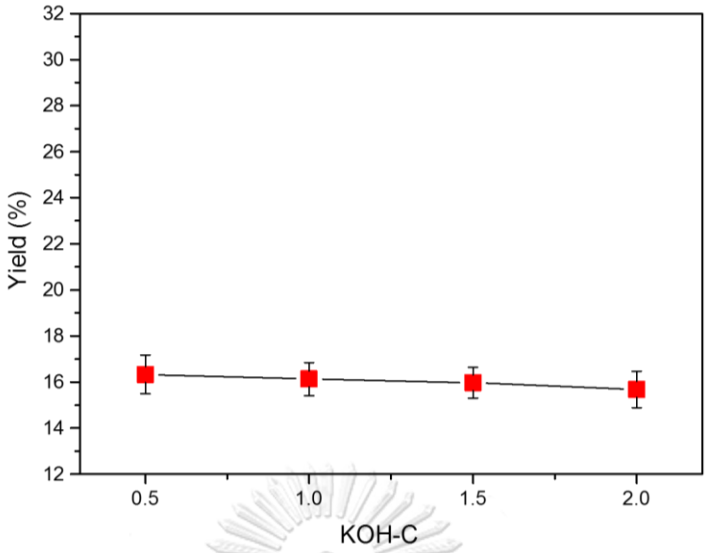

Figure 4.3 Production yield of AC products

The proximate and ultimate analysis of AC products produced from the various ratio of an activating agent showed in **Table. 4.3**. The proximate analysis revealed that the volatile matter content decreased with the increase in the KOH ratio due to volatile decomposition during the activation process. While the fixed carbon content significantly increased with the higher KOH ratio, which was in the range between 89.4-91.2%. In contrast, the ash content decreased due to the elimination of inorganic substances by alkali hydroxide treatment [41, 47]. The AC products contained a large amount of fixed carbon content, which was considered as AC materials, consisting of the fixed carbon content over 80% and low ash content of 2-10% [48]. The ultimate analysis results showed the C content greatly decreased with the increase in the KOH ratio owing to the collapse of carbon structure by reacting with alkali hydroxide. The H, O, and N content also reduced due to the oxidation reaction during the activation process. The AC products contained high C content of 69.5-79.8%, which was similar to the commercial AC, consisting of C content about 70% [49].

Table 4.3 Proximate and ultimate analysis of activated carbon products

Sample	Moisture (wt%)	Volatile (wt%)	Fixed carbon (wt%)	Ash (wt%)	C (wt%)	H (wt%)	N (wt%)	O (wt%)
HFO	10.2	57.2	31.7	0.9	64.9	7.8	9.2	18.1
C-700	3.4	8.1	83.8	4.7	86.8	1.9	0.7	10.6
AC-0.5:1	3.1	4.7	84.7	7.5	79.8	0.5	0.9	18.8
AC-1:1	3.7	3.9	87.1	5.3	79.2	0.4	0.6	19.8
AC-1.5:1	4.4	3.1	88.6	3.9	73.1	1.1	0.6	25.2
AC-2:1	5.7	2.9	90.2	1.2	69.5	1.2	0.7	28.6

Fig. 4.4 illustrates the morphology of AC products obtained at the KOH ratio of 0.5, 1, 1.5, and 2. The AC products exhibited the best pore development, which was a large number of porous structures. Also, more cavities were created resulted from the interaction between carbon atoms and KOH during the activation process. The results confirmed the release of organic substances in the carbonization combined with KOH activation process. As showed in **Fig. 4.4b**, a well-developed porous structure was created under the condition of 1:1 (KOH:HFO). However, the destroy of porous structure could be observed when the KOH ratio was higher than one (**Fig. 4.4c-d**) owing to the excessive amount of KOH. Therefore, the AC obtained from the KOH activation in the ratio of 1:1 was the most suitable for catalyst support.

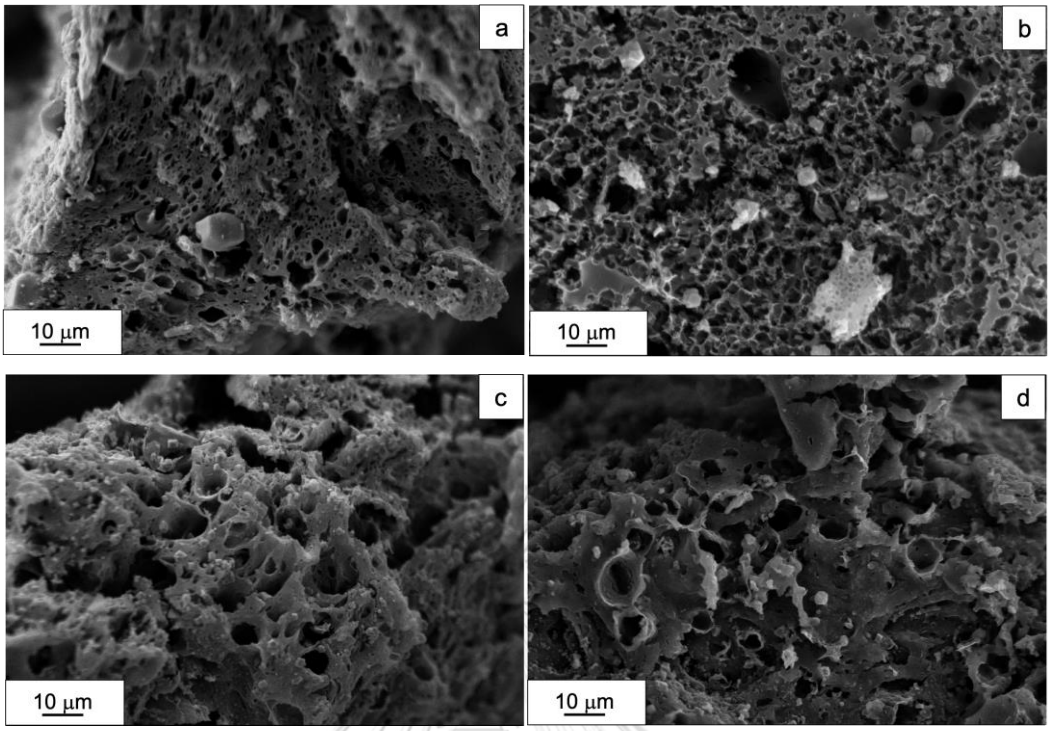

Figure 4.4 SEM micrographs of AC product (a) AC-0.5:1, (b) AC-1:1, (c) AC-1.5:1 and (d) AC-2:1

Table. 4.4 shows the surface properties of AC products obtained from the activation with different activating agent ratios. The AC exhibited BET surface area (S_{BET}), total pore volume (V_T), and micropore volume (V_{mi}) higher than the carbonized products, indicating the pore development resulted from alkali hydroxide treatment during the activation process. The surface area and pore volume of AC was increased with the KOH ratio was increased from 0.5 to 1. However, the surface area and pore volume consistently decreased when the ratio of KOH greater than unity resulted from the destruction of porous structures due to the excessive number of KOH. The maximum surface area and total pore volume were 1527.4 m^2/g and 0.758 cm^3/g, respectively obtained from the KOH activation in the ratio of 1:1. The N_2-physisorption isotherm of AC with the optimum condition revealed in **Fig. 4.5**. The sample displayed characteristics of mixed type I and IV isotherm, according to the International Union of Pure and Applied Chemistry (IUPAC) [17, 48]. The isotherm exhibited a steep slope at low relative pressure, corresponding to the microporous structure and a width hysteresis loop at high relative pressure, corresponding to the mesoporous structure. Also, the pore

size distribution confirmed the uniform porous structures with a diameter of 1.8-4.2 nm, as showed in **Fig. 4.5**. It was relating to the results of SEM images, which displayed the formation of micro- and mesoporous structures. The results suggested that the KOH activation significantly affected the properties of AC products, which possessed high surface area and large pore volume.

Table 4.4 Surface properties of AC products

Sample	S_{BET} (m^2/g)	V_T (cm^3/g)	V_{mi} (cm^3/g)	D_{avg} (nm)
C-700	48.6	0.051	0.003	4.2
AC-05:1	1017.4	0.576	0.244	2.0
AC-1:1	1527.4	0.758	0.477	1.8
AC-1.5:1	1426.5	0.711	0.384	1.8
AC-2:1	1308.1	0.669	0.191	1.8

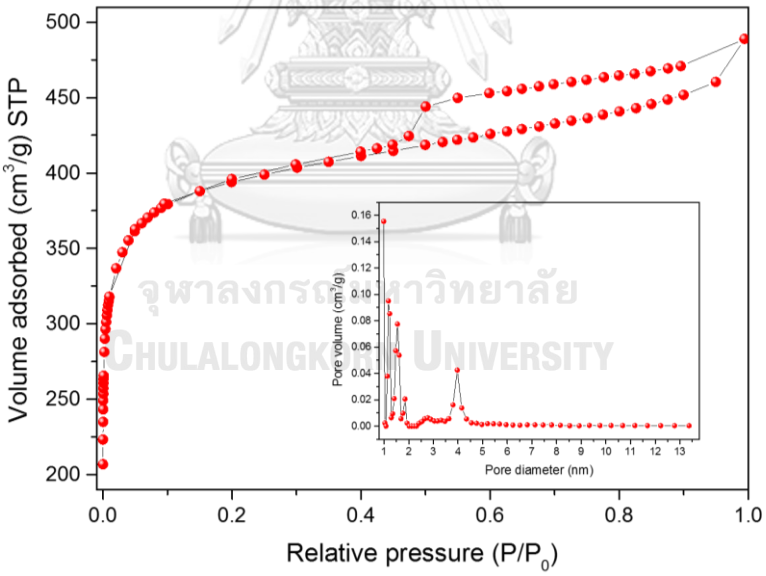

Figure 4.5 N_2-sorption isotherms and pore size distribution of AC (AC-1:1)

Additionally, the FTIR technique was used to identify chemical bonds and surface functional groups of AC products, The FTIR spectra of blank sample and AC products showed in **Fig. 4.6**, all spectra depended on the nature of the HFO precursor and synthesis method. The important bands of the blank sample located at 2920 and

2850 cm^{-1} were attributed to the -C-H stretching vibration presented in the alkane group [49]. The bands located at 1460 and 1370 cm^{-1} were ascribed to the -C-H bending vibration presented in the alkane group [50]. Thus, the results confirmed functional groups of the HFO, which mainly consisted of carbon atoms bond with H and O. In the case of AC, the FTIR spectra could not be observed due to the thermal decomposition of organic substances, which was complete oxidation of H and O atoms. Furthermore, the FTIR of the resultant AC was similar to the commercial AC, which could be confirmed products mainly consisted of carbon.

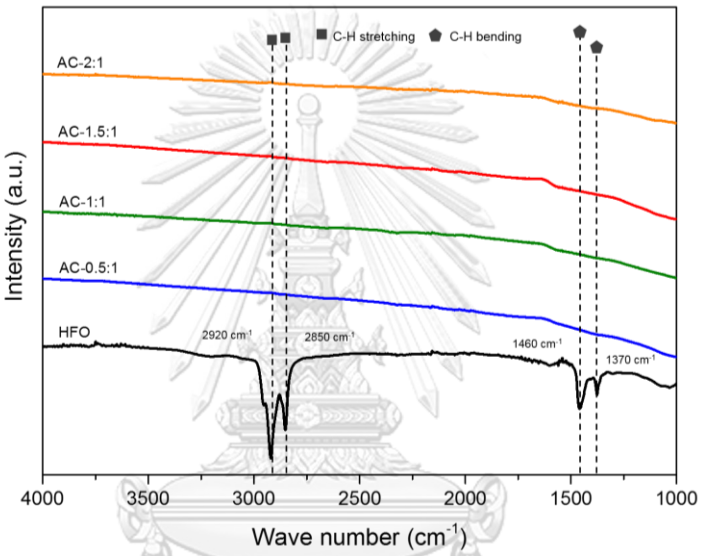

Figure 4.6 FTIR spectra of AC products

As described above, this study suggested the production of AC with high surface characteristics via the carbonization-chemical activation process. The BET surface area and pore volume of 1527.4 m^2/g and 0.758 cm^3/g, respectively, obtained from activation in the ratio of 1:1 (KOH:HFO) and carbonization at 700°C. The produced AC had a high carbon content of 87.1% with low ash content. The AC was possibly used as catalyst support for application in the HDO process. Furthermore, the preparation of the MoP catalyst and the catalytic performance in the HDO reaction were investigated and discussed further.

4.2 Preparation of molybdenum phosphide catalyst impregnated on AC

The MoP-AC catalyst was prepared by the wet-impregnation process using AC support. Also, the characteristics of the catalyst, which could be confirmed the formation of MoP on AC support (e.g., surface morphology, elemental composition, crystal structure, surface properties, acidity properties, and reducibility properties) were characterized. The effect of metal phosphide loading on AC support was analyzed to investigate the optimum condition of the MoP-AC catalyst.

4.2.1 Effect of metal phosphide loading

The surface morphology and elemental compositions of MoP-AC catalysts were characterized by a scanning electron microscope-energy dispersive spectrometry and a transmission electron microscope. **Fig. 4.7** shows the morphology and elemental composition of catalysts obtained at the MoP loading of 5, 10, 15, and 20 wt%. The results exhibited a well-dispersed with no-lump formation of metal nanoparticles, which was the uniform distribution of the MoP on AC support. Moreover, the presence of MoP particles on the support was confirmed by an elemental composition analysis, as showed in **Table 4.5**. The elemental contents of catalysts evaluated from the EDS technique were closed to the theoretical value (5, 10, 15, and 20 wt%), which revealed the evidence of MoP particles on AC support. Furthermore, the number of Mo and P increased with the increase in the MoP loading, indicating the successful impregnation of the MoP on the support.

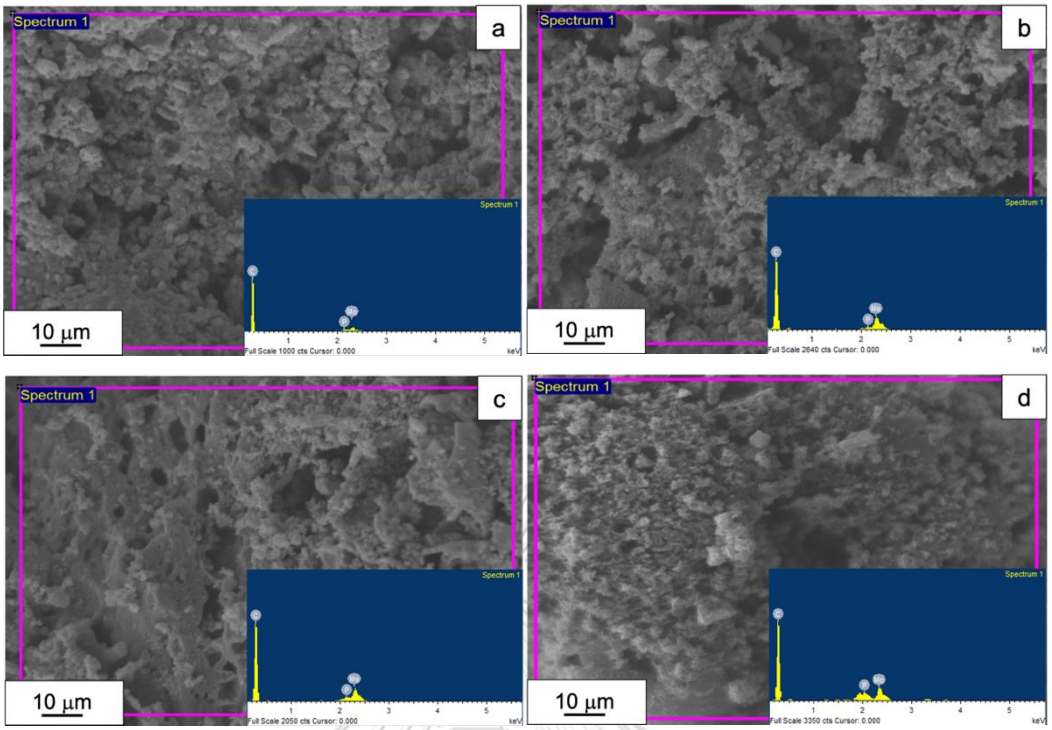

Figure 4.7 SEM micrographs of MoP catalyst (a) 5MoP-AC, (b) 10MoP-AC, (c) 15MoP-AC and (d) 20MoP-AC

Table 4.5 Elemental composition of MoP-AC catalysts

Catalyst	C K (wt%)	Mo L (wt%)	P K (wt%)
5MoP-AC	91.2	4.3	4.5
10MoP-AC	81.5	8.7	9.8
15MoP-AC	71.9	13.9	14.2
20MoP-AC	63.8	17.3	18.9

The morphology and particle size distribution of catalysts displayed in **Fig. 4.8**, it could be observed the MoP particles (dark spot) were well-dispersed on the surface of AC support (light area). The higher MoP loading led to the increase in the metal nanoparticles agglomeration, indicating the increase in black areas. It was corresponding to the particle size distribution (**Table 4.8**), which showed the larger average particle size as the MoP loading increased. The average particle size was shifted from 22.1 to 41.4 nm with the MoP loading was increased from 5 to 20 wt%,

respectively. Moreover, the rise in the MoP loading also caused the AC support collapse resulted in the aggregation of metal nanoparticles and the reduction in the specific surface area.

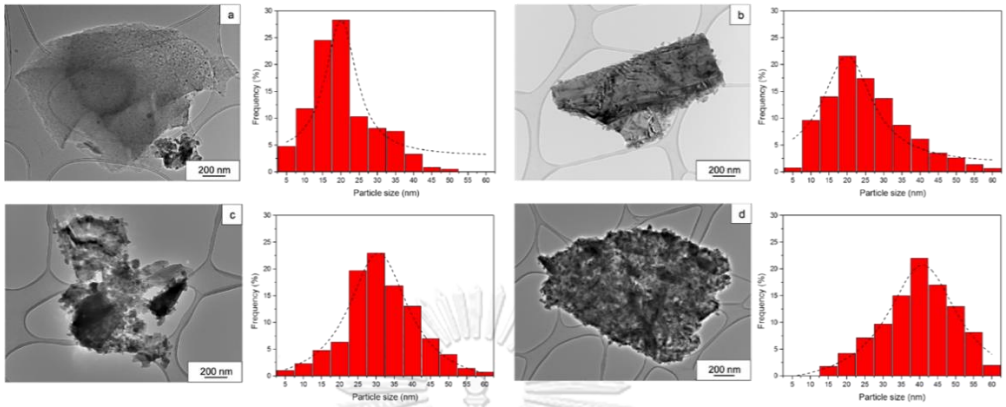

Figure 4.8 TEM micrographs and particle size distribution of MoP catalyst (a) 5MoP-AC, (b) 10MoP-AC, (c) 15MoP-AC and (d) 20MoP-AC

Table 4.6. shows the surface properties of catalysts obtained from the wet-impregnation with different initial metal phosphide loading. The catalysts exhibited BET surface area (S_{BET}), total pore volume (V_T), and micropore volume (V_{mi}) lower than there of the pristine AC support, indicating pore blocking by metal nanoparticles deposition. The surface area and pore volume of catalysts was decreased from 629.2 m^2/g and 0.307 cm^3/g to 423.1 m^2/g and 0.249 cm^3/g with the MoP loading was increased from 5 to 20 wt%, respectively, resulted from the erosion of porous structures due to agglomeration of metal nanoparticles. It was corresponding to the results of TEM images and particle size distribution, which revealed poor dispersion of the MoP on AC support and the increase in average particle size as the MoP loading increased. The N_2-physisorption isotherm and pore size distribution of the MoP-AC catalysts illustrated in **Fig. 4.9**. As showed in **Fig. 4.9a**, the physisorption curve coincided with type I and IV isotherm classified by the International Union of Pure and Applied Chemistry (IUPAC) [17, 48], which corresponding to micro- and mesoporous structures. The pore size distribution confirmed the presence of micro- and mesoporous structures with a diameter of 1.8-2.2 nm, as showed in **Fig. 4.9b**. Also, it could be observed the decrease of microporous structures after the impregnation of metal nanoparticles resulted from

the closure of porous structure, indicting the slightly increased in average pore diameter. This study suggested the amount of MoP loading was directly affected the distribution of MoP particles. Hence, the uniform dispersion of the MoP on AC support will provide good catalytic activity in the HDO reaction.

Table 4.6 Surface properties of MoP-AC catalysts

Sample	S_{BET} (m^2/g)	V_T (cm^3/g)	V_{mi} (cm^3/g)	D_{avg} (nm)
AC	1527.4	0.758	0.477	1.8
5MoP-AC	629.2	0.307	0.187	1.8
10MoP-AC	551.6	0.294	0.175	1.8
15MoP-AC	497.6	0.283	0.089	2.0
20MoP-AC	423.1	0.249	0.072	2.2

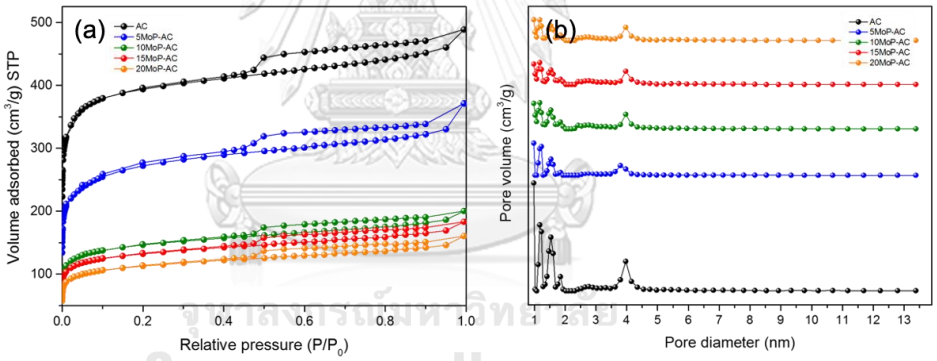

Figure 4.9 (a) N_2-sorption isotherm and (b) pore size distribution of MoP-AC catalysts

Basically, the XRD technique was commonly used to confirm the formation of the metal phosphide catalyst. **Fig. 4.10** demonstrates XRD patterns of MoP-AC catalysts, all patterns presented in the 2θ range of 10-80°. The samples exhibited high-intensity peak at 27.9, 32.1, 43.0, 57.2, 64.8, and 74.2, corresponding to the MoP phase [51, 52]. The intensity of peaks greatly decreased with the increase in the MoP loading, indicating the reduction in the crystallinity of catalysts resulted from the self-agglomeration of metal nanoparticles. Based on the Debye-Scherrer equation, the

crystalline size of MoP-AC catalysts was reported in **Table 4.7**. The average crystalline size was increased from 9.8 to 22.7 nm, with the MoP loading was increased from 5 to 20 wt%, respectively. It was corresponding to the results of TEM images and the N_2-physisorption technique, which revealed the increase in particle size and the decrease in specific surface area as the MoP loading increased. Thus, the crystallinity of resultant catalysts would probably affect the catalytic activity in the HDO reaction.

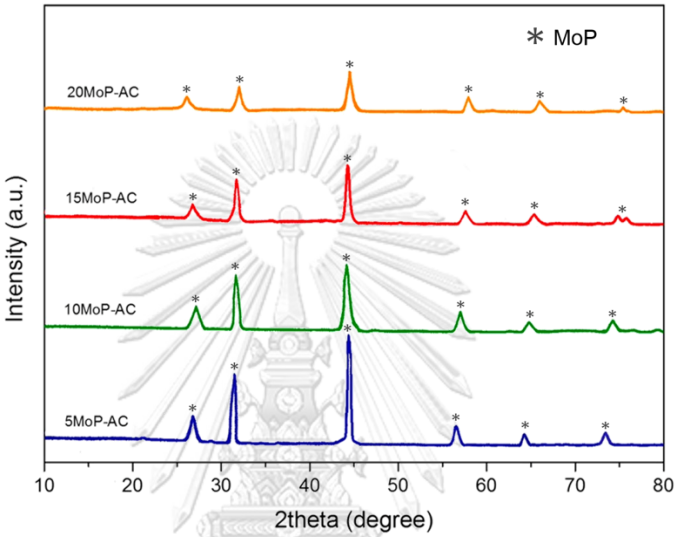

Figure 4.10 XRD patterns of MoP-AC catalysts

Table 4.7 The physical properties and acidity properties of MoP-AC catalysts

Catalyst	Particle size (nm)	Crystalline size (nm)	NH_3 uptake (mmol /g)
5MoP-AC	22.1	9.8	96.8
10MoP-AC	23.5	11.3	107.9
15MoP-AC	29.4	15.5	118.4
20MoP-AC	41.4	22.7	127.3

The acidity properties of MoP-AC catalysts were measured by using the ammonia temperature-programmed desorption technique. The NH_3-TPD profile of catalysts displayed in **Fig. 4.11**. The desorption of NH_3 which was observed at a temperature of 200-400°C, indicating the moderate strength acid site [53]. The

desorption peak related to the overlap contribution of the Brønsted and Lewis acid site. The Brønsted site was ascribed to the P-OH and Mo-OH groups, while the Lewis site would be associated with the electron-deficiency $Mo^{\delta+}$ species [54, 55]. The total NH_3 uptake of catalyst, which was measured from the peak area, was reported in **Table 4.7**. The NH_3 uptake was increased from 96.8 to 127.3 µmol/g, with the MoP loading was increased from 5 to 20 wt%, respectively, resulted from the rise in P contents, which was high Brønsted acid sites. Furthermore, the acidity properties of resultant catalysts will promote the deoxygenation as well as hydrocracking reaction [56].

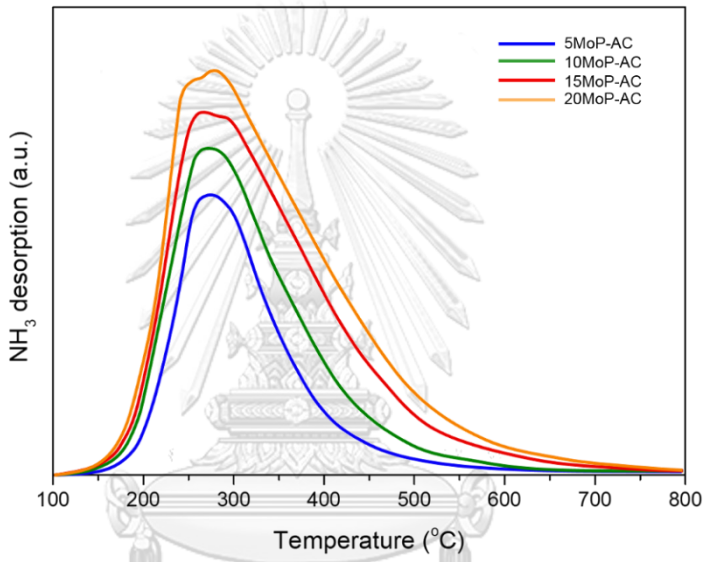

Figure 4.11 NH_3-TPD profiles of MoP-AC catalysts

Reducibility of MoP-AC catalysts were determined by using the hydrogen temperature-programmed reduction technique. The H_2-TPR profile of catalysts illustrated in **Fig. 4.12**. Higher consumption of H_2 in a temperature range 550-650°C could be observed, corresponding to the reduction of metal oxide to form metal phosphide. The consumption peak could be attributed to the co-reduction of MoO_2 (Mo^{4+} to Mo) and PO_x ($P^{\delta+}$ to P) [53]. During the TPR, the MoO_2 species were first reduced, then the H_2 dissociation from metallic Mo subsequently reduced PO_x species. Metallic Mo and P were bonded together to form MoP. The H_2 consumption peak slightly shifted to the lower temperature with the increase in the MoP loading, indicating the reduction of metal oxide was enhanced, relating to the poorly dispersed

of MoP nanoparticles on AC support and weak interaction between Mo and P species [57]. It was corresponding to the results of TEM images, N_2-physisorption, and XRD technique, which revealed poor dispersion of MoP with large particle size on AC support and the decrease in specific surface area as the MoP loading increased. The study suggested that the optimum reduction temperature was 600°C, which can be confirmed the complete reduction of such catalysts. Furthermore, resultant catalysts were reduced at 600°C for 3 h under the H_2 atmosphere to obtain the MoP form before study the HDO reaction.

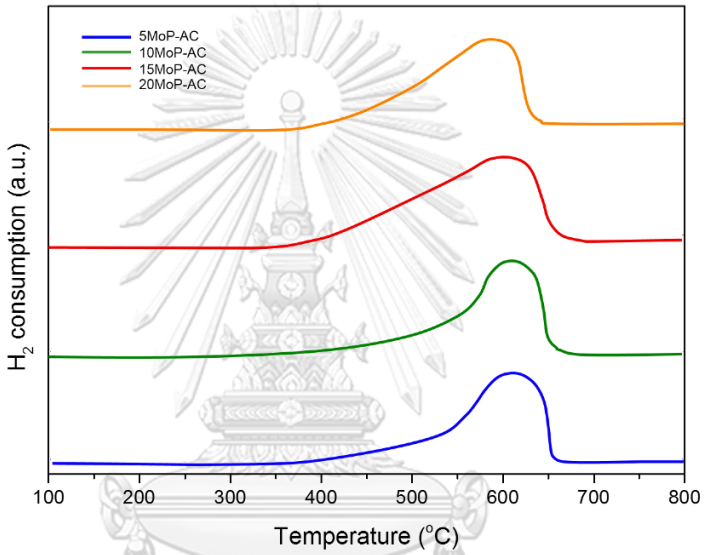

Figure 4.12 H_2-TPR profiles of MoP-AC catalysts

As described above, this study attained the preparation of the MoP catalyst impregnated on AC support via the wet-impregnation process. The results revealed the successful impregnation of MoP particles with a grain-like structure on AC support. The dispersion of metal nanoparticles and specific surface area decreased, as the MoP loading increased. The amount of MoP loading would strongly influence catalyst properties and activity. Therefore, the performance of the catalyst in the HDO reaction was examined and discussed.

4.3 Reaction study in HDO process

The catalytic activity was evaluated by the HDO of vegetable oil to produce green diesel and bio jet-oil. The effect of metal phosphide loading and reaction

temperature on catalytic performance (e.g., oil conversion, liquid HC yield, green diesel and, bio jet-oil selectivity) was examined. The bio jet-oil compositions in terms of C number and HC structure and %contribution of HDO and DCO/DCO_2 was also investigated. Furthermore, the long-term stability of the optimum catalyst was investigated based in the catalyst deactivation.

4.3.1 Effect of metal phosphide loading

As described above, the amount of metal phosphide loading on AC support will significantly affect the catalytic activity. The catalysts with various MoP loading were tested in the HDO of vegetable oil at a temperature of 400°C, H_2 pressure of 50 bar, LSHV = 1 h^{-1}, and H_2/oil ratio of 1000 N cm^3/cm^3. **Fig. 4.13** shows the effect of MoP loading on oil conversion, liquid HC yield, green diesel, and bio jet-oil selectivity. The results exhibited the catalytic activity with oil conversion of 100% could be achieved with all catalysts. However, the liquid HC yield was decreased from 66.4 to 61.1%, with the MoP loading was increased from 5 to 20 wt%, respectively, due to lower catalytic activity. The vegetable oil precursor was incompletely converted to liquid HC product. Also, the bio jet-oil (C_{9-14}) selectivity was decreased from 69.8 to 52.4%, with the MoP loading was increased from 5 wo 20 wt%, respectively owing to the low hydrocracking activity resulted from the worse surface characteristics of the resultant catalysts. During the reaction, MoP particles had less reaction capability resulted from large particle size and low crystallinity. It was corresponding to the results of TEM images, N_2-physisorption, XRD, and H_2-TPR technique, which revealed poor distribution of MoP with massive particle and crystalline size on AC support. Weak interaction between Mo and P would be supposed as the MoP loading increase. The results suggested the catalysts with the lower MoP loading exhibited higher activity in the HDO process, which provided high liquid HC yield and bio jet-oil selectivity. Based on all of mentioned results, it could be confirmed the 5MoP-AC was the optimum catalyst in this study.

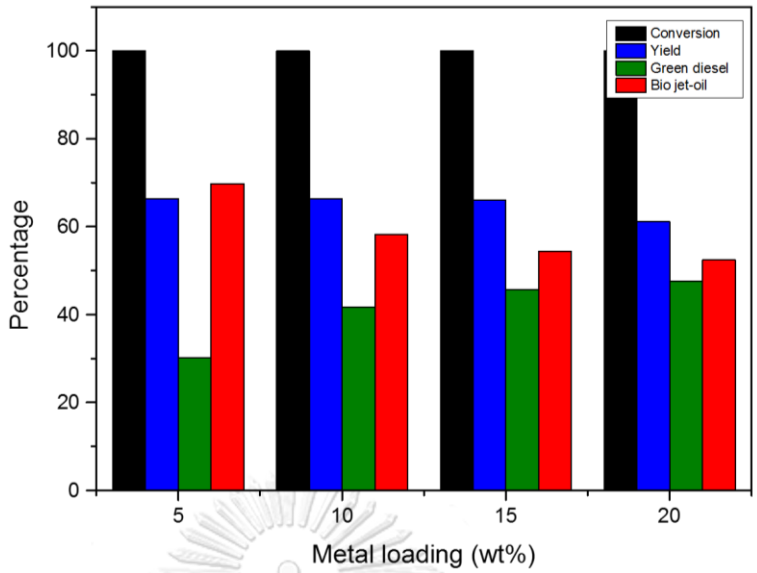

Figure 4.13 Effect of metal phosphide loading on oil conversion, liquid HC yield, green diesel and bio jet-oil selectivity of MoP-AC catalysts

Fig. 4.14 shows detailed compositions of bio jet-oil in terms of C number and %contribution of HDO and DCO/DCO_2. The results revealed that the short-chain HC was dominant products, indicating the hydrocracking reaction of long-chain HC to short-chain HC occurred in the operating condition. The amount of short-chain HC decreased with the increase in the MoP loading owing to the low hydrocracking activity resulted from the worse surface properties of the catalysts. Moreover, the decarbonylation (DCO) and decarboxylation (DCO_2) were dominant pathways with the presence of odd chain HC in products, suggesting the reactants were deoxygenated through the DCO and DCO_2 reactions, which CO and CO_2 was generated as by-products [12, 58]. Also, the detailed composition of bio jet-oil in terms of HC structure illustrated in **Fig. 4.15**. The results showed the paraffin HC (i.e., n-paraffin, iso-paraffin, and cyclo-paraffin) with a high-quality fuel was predominant products. The paraffin HC decreased with the increase in the MoP loading, while olefin and aromatic increased owing to the low deoxygenation activity resulted from poorly surface characteristics of the catalysts. However, the presence of oxygenated compounds (i.e., olefin and aromatic) under the condition of high MoP loading could be observed.

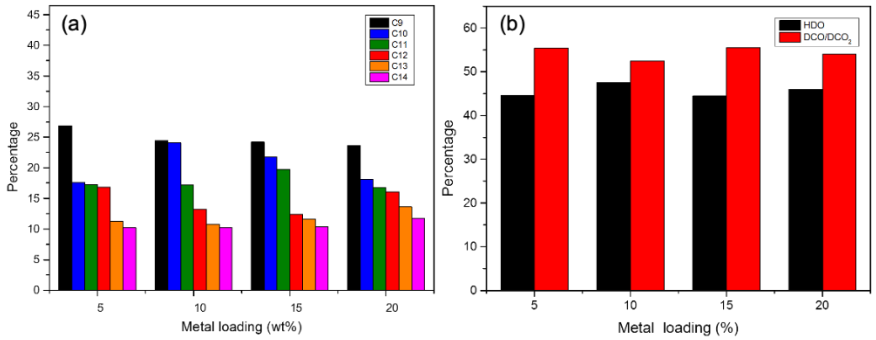

Figure 4.14 Effect of metal phiosphide loading on (a) bio jet-oil compositions in terms of C number and (b) %contribution of HDO and DCO/DCO_2 of MoP-AC catalysts

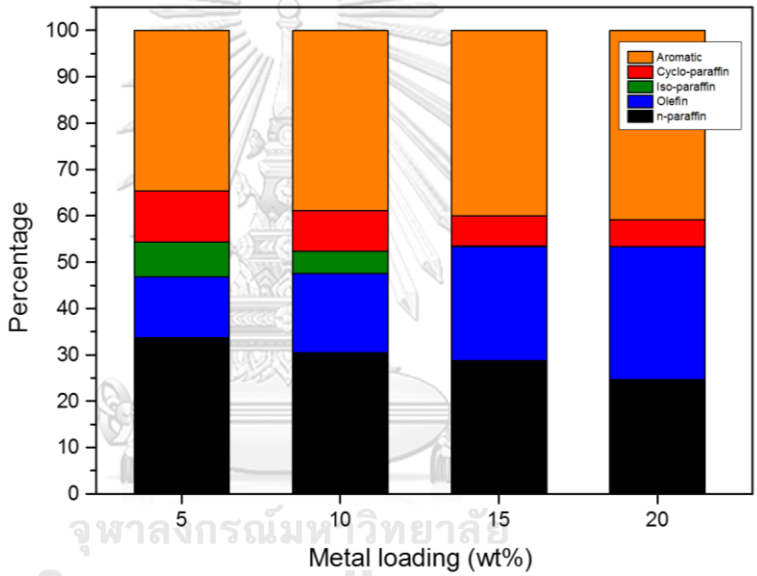

Figure 4.15 Effect of metal phosphide loading on bio jet-oil compositions in terms of HC structure of MoP-AC catalysts

4.3.2 Effect of reaction temperature

Basically, the reaction temperature strongly influenced on the catalytic activity, especially the hydrocracking and isomerization reactions [59]. The optimum temperature in the HDO reaction was investigated using the 5MoP-AC catalyst at temperatures of 400, 420, and 440°C. **Fig. 4.16** shows the effect of reaction temperature on oil conversion, liquid HC yield, green diesel, and bio jet-oil selectivity. The results demonstrated the catalytic performance with oil conversion up to 100% could be

obtained with all temperatures. The liquid HC yield was significantly decreased from 66.4 to 29.6%, with the reaction temperature was increased from 400 to 440°C, respectively resulted from the thermal decomposition of reactants and its intermediates during the HDO process. Otherwise, the bio jet-oil (C_{9-14}) selectivity increased from 69.8 to 92.4%, with the reaction temperature was increased from 400 to 440°C, respectively, owing to the hydrocracking reaction of long-chain HC to short-chain HC, which was favored at higher temperature [60, 61]. As showed in **Fig. 4.16** bio jet-oil selectivity of the condition of 420 and 440°C was quite similar (90.4 and 92.5%), while liquid HC yield of the condition of 440°C was meager (29.6%). The results suggested that the reaction temperature was directly affected the product yield and product selectivity. Thus, the optimum reaction temperature in this study was 420°C, which possessed high liquid HC yield and bio jet-oil selectivity.

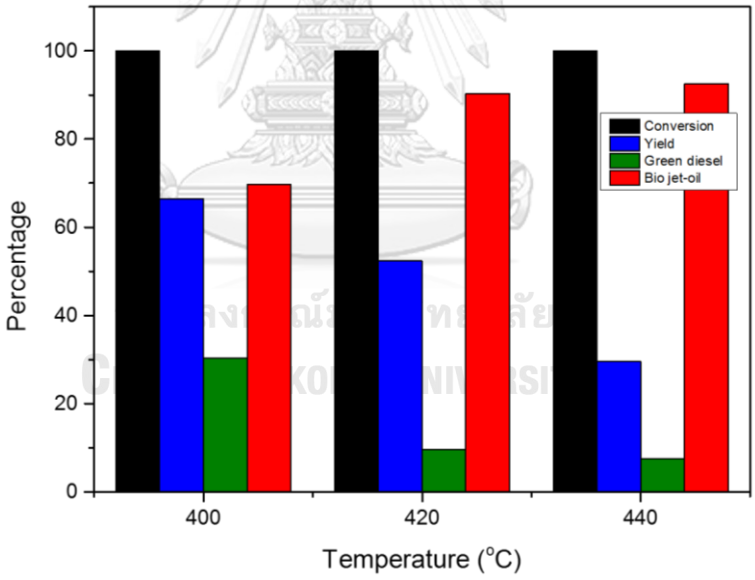

Figure 4.16 Effect of reaction temperature on oil conversion, liquid HC yield, green diesel and bio jet-oil selectivity of 5MoP-AC catalyst

Fig. 4.17 illustrates detailed compositions of bio jet-oil in terms of C number and %contribution of HDO and DCO/DCO_2. The results showed that the short-chain HC increased with the increase in the reaction temperature due to the high hydrocracking activity, which well-occurred at higher temperature, indicating long-

chain HC was forcefully converted to short-chain HC. The decarbonylation (DCO) and decarboxylation (DCO_2) were favored reactions in this study, which provided odd chain HC in products. The detailed composition of bio jet-oil in terms of HC structure displayed in **Fig. 4.18**. The results revealed the paraffin HC (i.e., n-paraffin, iso-paraffin, and cyclo paraffin) increased with the increase in the reaction temperature, while olefin and aromatic decreased owing to the high deoxygenation and isomerization activity. Therefore, the reduction of oxygenated compounds (i.e., olefin and aromatic) could be observed at higher temperature. **Table 4.8** compared the catalytic activity of as-prepared catalyst in the HDO of vegetable oil with other works. The results suggested the prepared catalyst displayed high catalytic activity with the oil conversion of 100%, which was similar to noble metal catalysts. Moreover, the bio jet-oil selectivity of the prepared catalyst was very high due to the operation at higher temperature, resulting in a high hydrocracking activity. Therefore, the prepared catalyst could be used instead of noble metal catalysts, which can be reduced economic drawbacks and achieved high-quality fuel.

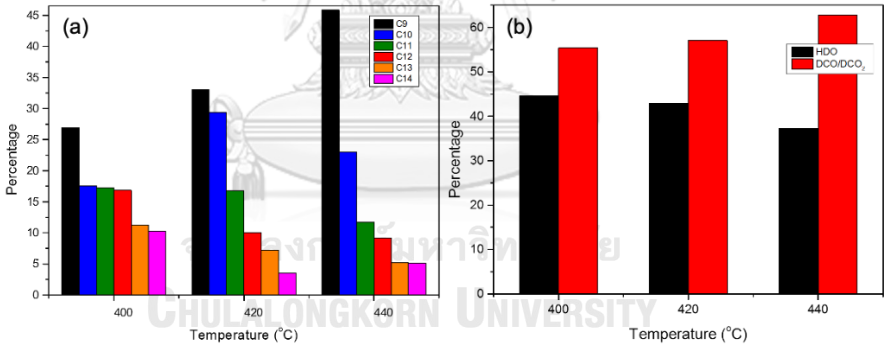

Figure 4.17 Effect of metal phiosphide loading on (a) bio jet-oil compositions in terms of C number and (b) %contribution of HDO and DCO/DCO_2 of 5MoP-AC catalyst

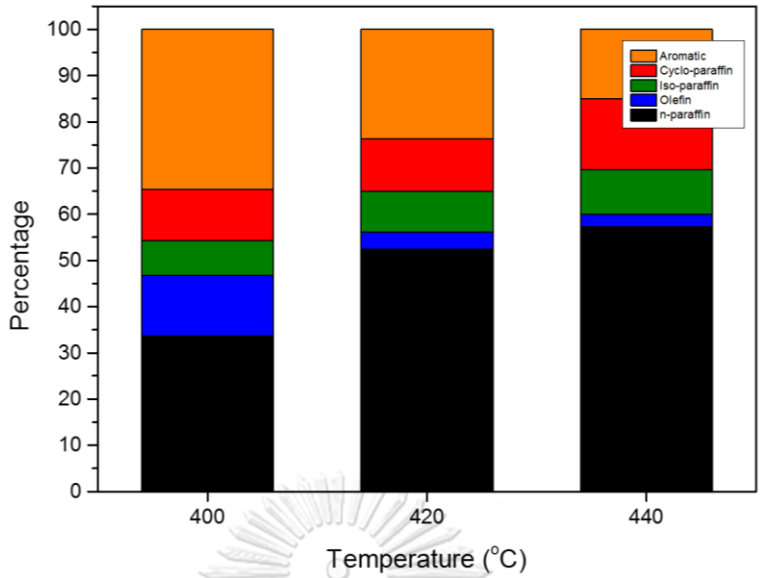

Figure 4.18 Effect of metal phosphide loading on bio jet-oil compositions in terms of HC structure of 5MoP-AC catalyst

Table 4.8 The HDO of vegetable oil to produce clean diesel

Feed	Catalyst	P (bar)	T (°C)	Reactor	Conversion	Jet selectivity	Ref
Palm oil	5Pd-Al_2O_3	50	330	Trickle-bed	100	36.1	[62]
Palm oil	5Pt-Al_2O_3	50	330	Trickle-bed	100	34.5	[62]
Date pits oil	4Pd-C	10	300	Batch	100	30.9	[4]
Date pits oil	4Pt-C	10	300	Batch	100	28.3	[4]
Palm oil	4Pd-C	40	400	Batch	100	49.1	[63]
Methly laurate	15MoP-Si_2O	20	300	Trickle-bed	86	98.7	[38]
Palm oil	5MoP-AC	50	420	Trickle-bed	100	90.4	-

4.3.3 Long-term stability test

Generally, a highly active and stable catalyst becomes economically advantageous in the industrial process. The long-term stability of the 5MoP-AC catalyst was evaluated in the HDO process at a temperature of 420°C and maintained continuously for 24 h. The catalytic performance, which was measured in terms of oil conversion and bio jet-oil selectivity illustrated in **Fig. 4.19**. After a continuous period run of 12 h on stream, the catalyst exhibited high catalytic activity as a stable conversion of 100%. It could be confirmed the poison (e.g., water and carbon) resistance of the resultant catalyst. The bio jet-oil selectivity was slightly decreased from 90.4 to 89.2% after 12 h on stream resulted from the reduction in catalytic activity. The results suggested the catalyst deactivation due to the coke formation, which was generated from carbon-based precursors and liquid HC products [64]. Thus, the 5MoP-AC catalyst's stability reached the conversion of 100% with bio jet-oil selectivity of 89.2% after 12 h on stream.

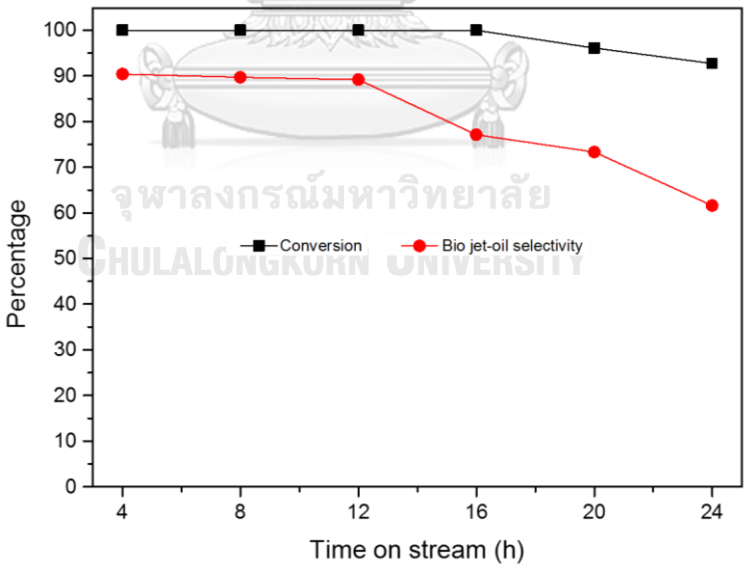

Figure 4.19 Long-term catalytic stability test of 5MoP-AC catalyst

As described above, this study was successful in the preparation of the MoP-AC catalyst impregnated on AC support. The catalysts can be applied in the HDO of

vegetable oil to produce clean fuel. The MoP loading of 5 wt% and a reaction temperature of 420°C was the optimum condition in this study, which provided 52.4 and 90.4% of liquid HC yield and bio jet-oil selectivity, respectively. Furthermore, the catalyst exhibited excellent catalytic performance with 89.2% bio jet-oil selectivity after 12 h on stream. The results suggested the HFO can be utilized as an active material for the production of an efficient catalyst in the HDO process.

CHAPTER 5
CONCLUSION

The experimental results reported in chapter 4, which consists of synthesis of activated carbon, preparation of molybdenum phosphide catalyst impregnated on AC, and reaction study in the hydrodeoxygenation process, were summarized. The experimental variables and optimum conditions were also reported. Moreover, other suggestions related to this research, which would be useful for future studies were described in this chapter.

5.1 Conclusion

5.11 Synthesis of activated carbon

The successful synthesis of activated carbon (AC) from heavy fuel oil (HFO) via the carbonization-chemical activation process with the production yield of 15.9% could be confirmed. The results suggested that the carbonization temperature affected AC properties when compared to the activating agent ratio. AC with a high surface area of 1524.7 m^2/g was obtained from KOH-activation with the ratio of 1:1 (KOH:HFO), and the carbonization temperature of 700°C. The produced AC had a high carbon content of 87.1% with low ash content. Moreover, it was observed the uniform porous structure, with an average pore diameter of 1-5 nm. Thus, the produced AC was applied as molybdenum phosphide (MoP) catalyst support for the hydrodeoxygenation (HDO) reaction.

5.12 Preparation of molybdenum phosphide catalyst impregnated on AC

The preparation of the molybdenum phosphide (MoP) catalyst impregnated on AC via the wet-impregnation process was confirmed. The microscopic analysis revealed the uniform dispersion of MoP nanoparticles with a grain-like structure on the support. The decreased in the specific surface of AC from 1527.4 to 629.2 m^2/g was also detected after impregnation with 5 wt% of MoP catalyst. The XRD results also confirmed the formation of MoP nanoparticles, with an average particle size of 22.1 nm. Furthermore, the as-prepared catalyst exhibited moderate acidity property, which promoted the deoxygenation reaction in this study.

5.1.3 Reaction study in HDO process

The as-prepared catalyst was employed in the HDO of vegetable oil to produce clean diesel. The results suggested that the amount of molybdenum phosphide loading affected catalytic activity when compared to the reaction temperature. The metal loading of 5 wt% and the reaction temperature of 420°C exhibited the best catalytic performance, with the oil conversion of 100%. The liquid HC consisted of 9.6 and 90.4% green diesel and bio jet-oil, respectively. Paraffin HC, in which high-quality fuel were dominant products, indicated high deoxygenation activity. The decarbonylation (DCO) and decarboxylation (DCO_2) reactions were favored in this study, with the presence of odd-chain HC in the product. Furthermore, the catalyst showed excellent stability for 12 h on stream without catalyst deactivation.

5.2 Recommendation

5.2.1 The other methods for heavy fuel oil (HFO) pretreatment should be studied to reduce the preparation time and the environmental impact.

5.2.2 The effect of carbonization-activation conditions (i.e., carbonization time, heating rate, gas flow rate, and other activating agents, etc.) should be examined.

5.2.3 The characterization of molybdenum phosphide (MoP) catalyst in other techniques (i.e., XPS, and CO chemisorption, etc.) should be studied.

5.2.4 The effect of other operating conditions (i.e., reaction time, H_2 pressure, gas flow rate, and LSHV, etc.) in the hydrodeoxygenation (HDO) reaction should be more examined.

5.2.5 The catalyst deactivation mechanism should be studied to prevent the deactivation of the further.

REFERENCES

VITA

NAME	Araya Smuthkochorn
DATE OF BIRTH	August 12, 1995
PLACE OF BIRTH	Bangkok, Thailand
INSTITUTIONS ATTENDED	Chulalongkorn University
HOME ADDRESS	Bangkok, Thailand
PUBLICATION	A. Smuthkochorn, A. Eiad-ua, K. Faungnawakij, T. Charinpanitkul, Production of activated carbon impregnated with monoethanolamine from cattail leaves for carbon dioxide adsorption, Proceedings of Joint Conference on Renewable Energy and Nanotechnology, (2018).
AWARD RECEIVED	Excellent Paper Award of JCREN 2018, Production of activated carbon impregnated with monoethanolamine from cattail leaves for carbon dioxide adsorption, 2018.

1. Vijayakumar, G. and A. Pandurangan, *Up-gradation of α-tetralone to jet-fuel range hydrocarbons by vapour phase hydrodeoxygenation over Pd Ni/SBA-16 catalysts.* Energy, 2017. **140**: p. 1158-1172.
2. Zecca, A. and L. Chiari, *Fossil-fuel constraints on global warming.* Energy Policy, 2010. **38**: p. 1-3.
3. Chu, P.L., et al., *Process modeling of hydrodeoxygenation to produce renewable jet fuel and other hydrocarbon fuels.* Fuel, 2017. **196**: p. 298-305.
4. Al-Muhtaseb, A.a.H., et al., *Efficient utilization of waste date pits for the synthesis of green diesel and jet fuel fractions.* Energy Conversion and Management, 2016. **127**: p. 226-232.
5. Silva, L.N., et al., *Biokerosene and green diesel from macauba oils via catalytic deoxygenation over Pd/C.* Fuel, 2016. **164**: p. 329-338.
6. Xu, J. and M. Li, *Innovative technological paradigm-based approach towards biofuel feedstock.* Energy Conversion and Management, 2017. **141**: p. 48-62.
7. Narowska, B., et al., *Use of activated carbons as catalyst supports for biodiesel production.* Renewable Energy, 2019. **135**: p. 176-185.
8. Gasparatos, A., et al., *Mechanisms and indicators for assessing the impact of biofuel feedstock production on ecosystem services.* Biomass and Bioenergy, 2018. **114**: p. 157-173.
9. Leong, W.-H., et al., *Third generation biofuels: A nutritional perspective in enhancing microbial lipid production.* Renewable and Sustainable Energy Reviews, 2018. **91**: p. 950-961.
10. Iisa, K., et al., *Production of low-oxygen bio-oil via ex situ catalytic fast pyrolysis and hydrotreating.* Fuel, 2017. **207**: p. 413-422.
11. Yang, T., et al., *Hydrodeoxygenation of crude bio-oil in situ in the bio-oil aqueous phase with addition of zero-valent aluminum.* Fuel Processing Technology, 2019. **184**: p. 65-72.
12. Cheng, F. and C.E. Brewer, *Producing jet fuel from biomass lignin: Potential pathways to alkyl-benzenes and cycloalkanes.* Renewable and Sustainable Energy Reviews, 2017. **72**: p. 673-722.

13. de Sousa, F.P., C.C. Cardoso, and V.M.D. Pasa, *Producing hydrocarbons for green diesel and jet fuel formulation from palm kernel fat over Pd/C.* Fuel Processing Technology, 2016. **143**: p. 35-42.
14. Wu, X., et al., *Catalytic upgrading of ethanol to n-butanol over M-CeO2/AC (M=Cu, Fe, Co, Ni and Pd) catalysts.* Catalysis Communications, 2017. **100**: p. 15-18.
15. Rashidi, N.A. and S. Yusup, *An overview of activated carbons utilization for the post-combustion carbon dioxide capture.* Journal of CO2 Utilization, 2016. **13**: p. 1-16.
16. Ameen, M., et al., *Catalytic hydrodeoxygenation of triglycerides: An approach to clean diesel fuel production.* Renewable and Sustainable Energy Reviews, 2017. **80**: p. 1072-1088.
17. Tsoncheva, T., et al., *Activated carbon from Bulgarian peach stones as a support of catalysts for methanol decomposition.* Biomass and Bioenergy, 2018. **109**: p. 135-146.
18. Zaky, M.T. and S.M. Tawfik, *Production of lubricating base oil from slop wax by different subsequent refining techniques.* Fuel Processing Technology, 2011. **92**(3): p. 447-451.
19. Li, W., et al., *Effects of carbonization temperatures on characteristics of porosity in coconut shell chars and activated carbons derived from carbonized coconut shell chars.* Industrial Crops and Products, 2008. **28**(2): p. 190-198.
20. Olcese, R., et al., *Gas-phase hydrodeoxygenation of guaiacol over iron-based catalysts. Effect of gases composition, iron load and supports (silica and activated carbon).* Applied Catalysis B: Environmental, 2013. **129**: p. 528-538.
21. Sathishkumar, P., M. Arulkumar, and T. Palvannan, *Utilization of agro-industrial waste Jatropha curcas pods as an activated carbon for the adsorption of reactive dye Remazol Brilliant Blue R (RBBR).* Journal of Cleaner Production, 2012. **22**(1): p. 67-75.
22. Zecca, A. and L. Chiari, *Fossil-fuel constraints on global warming.* Energy Policy, 2010. **38**(1): p. 1-3.
23. Tadda, M.A., et al., *A review on activated carbon: process, application and prospects*. Vol. 2. 2016. 7-13.

24. Lam, S.S., et al., *Microwave-assisted pyrolysis with chemical activation, an innovative method to convert orange peel into activated carbon with improved properties as dye adsorbent.* Journal of Cleaner Production, 2017. **162**: p. 1376-1387.

25. Foo, K.Y. and B.H. Hameed, *A short review of activated carbon assisted electrosorption process: An overview, current stage and future prospects.* Journal of Hazardous Materials, 2009. **170**(2): p. 552-559.

26. Ioannidou, O. and A. Zabaniotou, *Agricultural residues as precursors for activated carbon production—A review.* Renewable and Sustainable Energy Reviews, 2007. **11**(9): p. 1966-2005.

27. Zdravkov, B.D., et al., *Pore classification in the characterization of porous materials: A perspective.* Central European Journal of Chemistry, 2007. **5**(2): p. 385-395.

28. Pang, Y., et al., *Effect of Methane Adsorption on Stress-Dependent Porosity and Permeability in Shale Gas Reservoirs*. 2016.

29. Donohue, M.D. and G.L. Aranovich, *Classification of Gibbs adsorption isotherms.* Advances in Colloid and Interface Science, 1998. **76-77**: p. 137-152.

30. Basu, P., *Chapter 14 - Analytical Techniques*, in *Biomass Gasification, Pyrolysis and Torrefaction (Third Edition)*, P. Basu, Editor. 2018, Academic Press. p. 479-495.

31. Sielawa Brasil, D., et al., *Use of sugarcane bagasse and candeia waste for solid biofuels production*. Vol. 45. 2014. 185.

32. Sing, K., *The use of nitrogen adsorption for the characterisation of porous materials.* Colloids and Surfaces A: Physicochemical and Engineering Aspects, 2001. **187-188**: p. 3-9.

33. Jiang, W., et al., *Synthesis, characterization and machine learning based performance prediction of straw activated carbon.* Journal of Cleaner Production, 2019. **212**: p. 1210-1223.

34. Kacher, J., et al., *Bragg's Law diffraction simulations for electron backscatter diffraction analysis.* Ultramicroscopy, 2009. **109**(9): p. 1148-1156.

35. Rodríguez-González, L., et al., *The acid properties of H-ZSM-5 as studied by NH3-TPD and 27Al-MAS-NMR spectroscopy.* Applied Catalysis A: General, 2007. **328**(2): p. 174-182.
36. Reiche, M.A., M. Maciejewski, and A. Baiker, *Characterization by temperature programmed reduction.* Catalysis Today, 2000. **56**(4): p. 347-355.
37. Shi, H., et al., *Catalytic deoxygenation of methyl laurate as a model compound to hydrocarbons on nickel phosphide catalysts: Remarkable support effect.* Fuel Processing Technology, 2014. **118**: p. 161-170.
38. Alvarez-Galvan, M.C., et al., *Metal phosphide catalysts for the hydrotreatment of non-edible vegetable oils.* Catalysis Today, 2018. **302**: p. 242-249.
39. Hui, T.S. and M.A.A. Zaini, *Potassium hydroxide activation of activated carbon: a commentary.* Carbon letters, 2015. **16**(4): p. 275-280.
40. Huang, Y., E. Ma, and G. Zhao, *Thermal and structure analysis on reaction mechanisms during the preparation of activated carbon fibers by KOH activation from liquefied wood-based fibers.* Industrial Crops and Products, 2015. **69**: p. 447-455.
41. Gao, Y., et al., *Preparation of high surface area-activated carbon from lignin of papermaking black liquor by KOH activation for Ni(II) adsorption.* Chemical Engineering Journal, 2013. **217**: p. 345-353.
42. Sayed Ahmed, S.A., R.M.M. Abo El-Enin, and T. El-Nabarawy, 2009. **10**.
43. Mohammadi, S. and N. Mirghaffari, *A preliminary study of the preparation of porous carbon from oil sludge for water treatment by simple pyrolysis or KOH activation.* New Carbon Materials, 2015. **30**(4): p. 310-318.
44. Dizbay-Onat, M., U.K. Vaidya, and C.T. Lungu, *Preparation of industrial sisal fiber waste derived activated carbon by chemical activation and effects of carbonization parameters on surface characteristics.* Industrial Crops and Products, 2017. **95**: p. 583-590.
45. Gillespie, G.D., et al., *Prediction of quality parameters of biomass pellets from proximate and ultimate analysis.* Fuel, 2013. **111**: p. 771-777.
46. Klimov, O.V., et al., *Co–Mo catalysts for ultra-deep HDS of diesel fuels prepared via synthesis of bimetallic surface compounds.* Journal of Molecular Catalysis A: Chemical, 2010. **322**(1-2): p. 80-89.

47. El-Hendawy, A.-N.A., *An insight into the KOH activation mechanism through the production of microporous activated carbon for the removal of Pb2+ cations.* Applied Surface Science, 2009. **255**(6): p. 3723-3730.

48. Zhang, Y.-J., et al., *Effects of steam activation on the pore structure and surface chemistry of activated carbon derived from bamboo waste.* Applied Surface Science, 2014. **315**: p. 279-286.

49. Chai, M.N. and M.I.N. Isa, *The Oleic Acid Composition Effect on the Carboxymethyl Cellulose Based Biopolymer Electrolyte.* Journal of Crystallization Process and Technology, 2013. **03**(01): p. 1-4.

50. Kong, S., et al., *Influence of surface modification of SrFe12O19 particles with oleic acid on magnetic microsphere preparation.* Particuology, 2008. **6**(3): p. 185-190.

51. Song, T., et al., *A facile route for large-scale synthesis of molybdenum phosphide nanoparticles with high surface area.* Phosphorus, Sulfur, and Silicon and the Related Elements, 2017. **192**(11): p. 1159-1164.

52. Yao, Z., et al., *Molybdenum phosphide as a novel and stable catalyst for dry reforming of methane.* Catalysis Science & Technology, 2016. **6**(22): p. 7996-8004.

53. Shi, L., et al., *Effect of phosphorus modification on the catalytic properties of Mo-Ni/Al2O3 in the hydrodenitrogenation of coal tar.* Journal of Fuel Chemistry and Technology, 2015. **43**(1): p. 74-80.

54. Li, K., R. Wang, and J. Chen, *Hydrodeoxygenation of Anisole over Silica-Supported Ni2P, MoP, and NiMoP Catalysts.* Energy & Fuels, 2011. **25**(3): p. 854-863.

55. Yang, Y., J. Chen, and H. Shi, *Deoxygenation of Methyl Laurate as a Model Compound to Hydrocarbons on Ni2P/SiO2, Ni2P/MCM-41, and Ni2P/SBA-15 Catalysts with Different Dispersions.* Energy & Fuels, 2013. **27**(6): p. 3400-3409.

56. Yang, X. and L. Ni, *Synthesis of hybrid hydrogel of poly(AM co DADMAC)/silica sol and removal of methyl orange from aqueous solutions.* Chemical Engineering Journal, 2012. **209**: p. 194-200.

57. Zhu, H., *Pd/CeO2?TiO2 catalyst for CO oxidation at low temperature: a TPR study with H2 and CO as reducing agents.* Journal of Catalysis, 2004. **225**(2): p. 267-277.

58. He, Z. and X. Wang, *Hydrodeoxygenation of model compounds and catalytic systems for pyrolysis bio-oils upgrading.* Catalysis for Sustainable Energy, 2012. **1**.

59. He, S., et al., *Hydro-pyrolysis of lignocellulosic biomass over alumina supported Platinum, Mo2C and WC catalysts.* Frontiers of Chemical Science and Engineering, 2017. **12**(1): p. 155-161.

60. Liu, Y., et al., *Hydrotreatment of Vegetable Oils to Produce Bio-Hydrogenated Diesel and Liquefied Petroleum Gas Fuel over Catalysts Containing Sulfided Ni–Mo and Solid Acids.* Energy & Fuels, 2011. **25**(10): p. 4675-4685.

61. Wang, W., et al., *Preparation of NiS 2 //MoS 2 catalysts by two-step hydrothermal method and their enhanced activity for hydrodeoxygenation of p -cresol.* Fuel, 2016. **179**: p. 1-9.

62. Srifa, A., et al., *Roles of monometallic catalysts in hydrodeoxygenation of palm oil to green diesel.* Chemical Engineering Journal, 2015. **278**: p. 249-258.

63. Kiatkittipong, W., et al., *Diesel-like hydrocarbon production from hydroprocessing of relevant refining palm oil.* Fuel Processing Technology, 2013. **116**: p. 16-26.

64. Zhao, H.Y., et al., *Hydrodeoxygenation of guaiacol as model compound for pyrolysis oil on transition metal phosphide hydroprocessing catalysts.* Applied Catalysis A: General, 2011. **391**(1): p. 305-310.

APPENDIXS

APPENDIX A

RAW MATERIAL DATA

A.1 Specification data of heavy fuel oil (HFO)

Certificate No.: T-19/07952

Sample Lab No.: OP-FUO-1908473

Customer/Supplier: Bang Chak Petroleum Terminal, PTTOR PLC

Sample location: Depot: Bang Chak Petroleum Terminal, Tank No.: TA 01

Batch No.: TA 01/10/0004

Product source: Ship-SIRITABASIN, Refinery-REF-T

Received Date: 06 Mar 2019

Date of Test: 06 Mar 2019

Date of Sampling: 06 Mar 2019

Sample Condition: Normal

Table A.1 Specification of heavy fuel oil (HFO)

Test Item	Test Method	Limit	Result
1. API Gravity @60°F, Upper, °API	ASTM D 1298-12b	Report	17.8
2. API Gravity @60°F, Lower, °API	ASTM D 1298-12b	Report	17.5
3. Specific Gravity 15.6/15.6°C, Upper	ASTM D 1298-12b	Max. 0.985	0.9478
4. Specific Gravity 15.6/15.6°C, Lower	ASTM D 1298-12b	Max. 0.985	0.9497
5. Flash point (P.M.), °C	ASTM D 93-16a (Procedure B)	Min. 60	75.0
6. Kinematic Viscosity at 50°C, Upper, mm^2/s	ASTM D 445-17a	7-80	66.22
7. Kinematic Viscosity at 50°C, Lower, mm^2/s	ASTM D 445-17a	7-80	61.70
8. Sulfur Content, % wt.	ASTM D 2622-16	Max. 2.0	1.99(a)
9. Pour point, °C	ASTM D 5950-14	Max. 24	0(b)
10. Water and Sediment, % V/V	ASTM D 1796-04 (Reapproved 2009)	Max. 1.0	0.10
11. Ash Content, % wt.	ASTM D 482-07	Max. 0.1	0.28(b)
12. Micro Carbon Residue, % wt.	ASTM D 4503-06E1	Report	11.4(b)
13. Carbon, % mass	ASTM D 5291-02	Report	83.52(b)
14. Nitrogen, % mass	ASTM D 5291-02	Report	0.28(b)

15. Hydrogen, % mass	ASTM D 5291-02	Report	11.52(b)
16. Gross Heat of combustion, Btu/lb	ASTM D 4868-00 (Calculation)	Min. 18,000	18,610

Remark: *Test marked “Not TISI Accredited” in this Certificate are not included in the TISI Accreditation Schedule for our Laboratory

(a) Extracted from COA Sample Lab No. OP-FUO-1904922 tested on 05 Mar 2019.

(b) These tests are performed on monthly basis. Extracted from COA sample Lab No. OP-FUO-1904446 tested on 04 Feb 2019

A.2 Thermal behavior of heavy fuel oil (HFO)

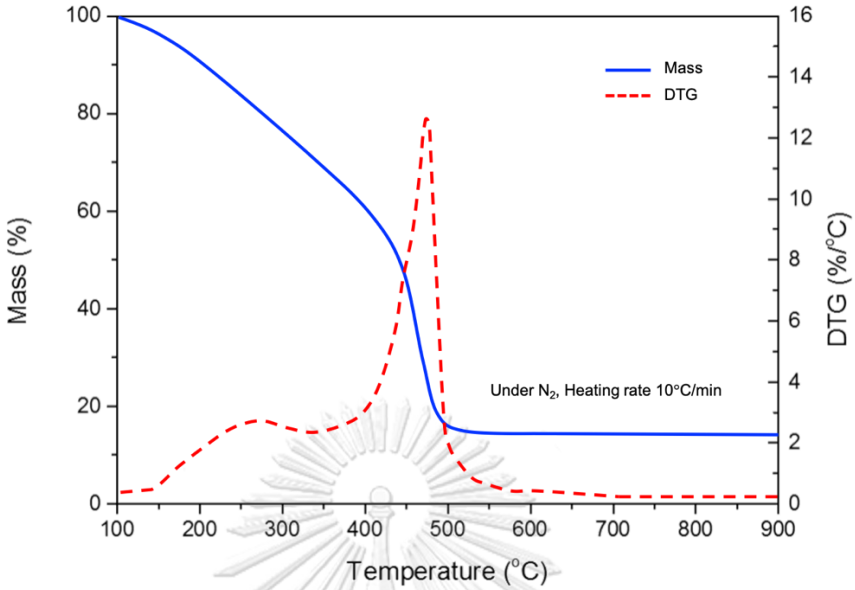

Figure A.1 TG/DTG analysis of heavy fuel oil (HFO)

APPENDIX B

TEMPERATURE PROFILE

B.1 Temperature profile of quartz horizontal tube reactor

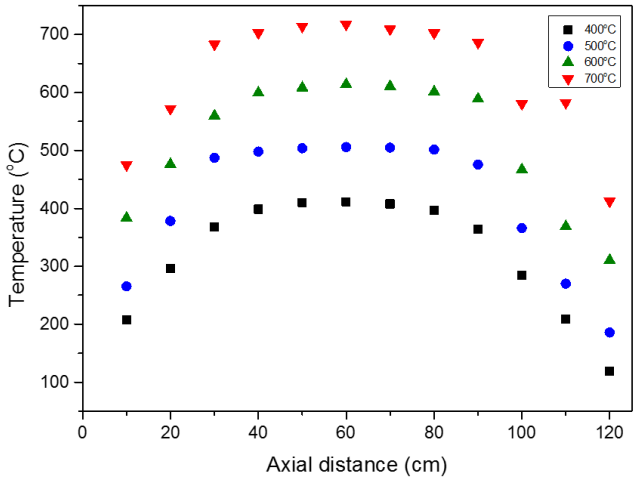

Figure B.1 Temperature profile of quartz horizontal tube reactor
Energy used: 4,000 kW/h.

B.2 Temperature profile of continuous-flow trickle-bed reactor

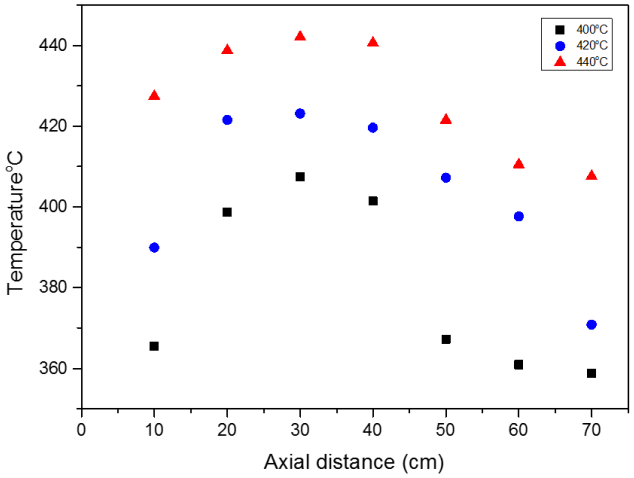

Figure B.2 Temperature profile of continuous-flow trickle-bed reactor
Energy used: 4,000 kW/h.

APPENDIX C

BASIC CALCULATION

C.1 Production yield of activated carbon (AC)

$$Yiled\ of\ AC\ (\%) = \frac{m_f}{m_0}\ x\ 100$$

Where:

m_f = mass of produced AC

m_0 = mass of HFO feedstock

C.2 Liquid hourly space velocity (LSHV)

$$LSHV\ (h^{-1}) = \frac{liquid\ volume\ flow\ per\ hour}{catalyst\ volume}$$

In this study: LSHV = 1 h^{-1}

$$LSHV\ (h^{-1}) = \frac{0.134\ ml \cdot\ min^{-1}}{8\ ml}\ x\ 60\ min$$

$$\therefore\ LSHV = 1.005\ h^{-1}$$

C.3 Oil conversion, liquid HC yield, green diesel, bio jet-oil selectivity, and %contribution of HDO and DCO/DCO_2

$$Oil\ conversion\ (\%) = \frac{m_0 - m_f}{m_0} x\ 100$$

$$Liquid\ HC\ yield\ (\%) = \frac{m_f}{m_0}\ x\ 100$$

$$Green\ diesel\ selectivity\ (\%) = \frac{m_{green\ diesel}}{m_{oil\ converted}} x\ 100$$

$$Bio\ jet\text{-}oil\ selectivity\ (\%) = \frac{m_{bio\ jet-oil}}{m_{oil\ converted}} x\ 100$$

$$HDO\ (\%) = \frac{m_{even\ number}}{m_{oil\ converted}} x\ 100$$

$$DCO/DCO_2\ (\%) = \frac{m_{odd\ number}}{m_{oil\ converted}} x\ 100$$

Where:

m_0 = mass of feed oil

m_f = mass of produced oil

$m_{green\ diesel}$ = mass of green diesel fraction

$m_{bio\ jet\text{-}oil}$ = mass of bio jet-oil fraction

$m_{even\ number}$ = mass of even number fraction

$m_{odd\ number}$ = mass of odd number fraction

APPENDIX D

PRODUCT COMPOSITION DATA

D.1 Product compositions obtained from the carbonization process

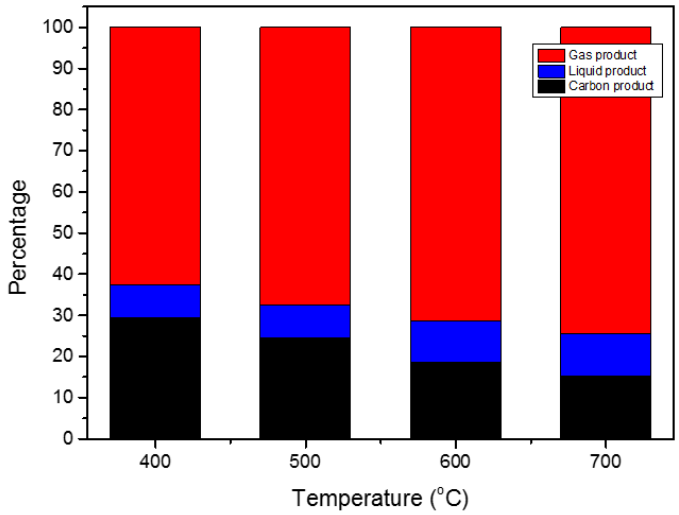

Figure D.1 Effect of carbonization temperature on product compositions
Liquid product: Moisture and Tar

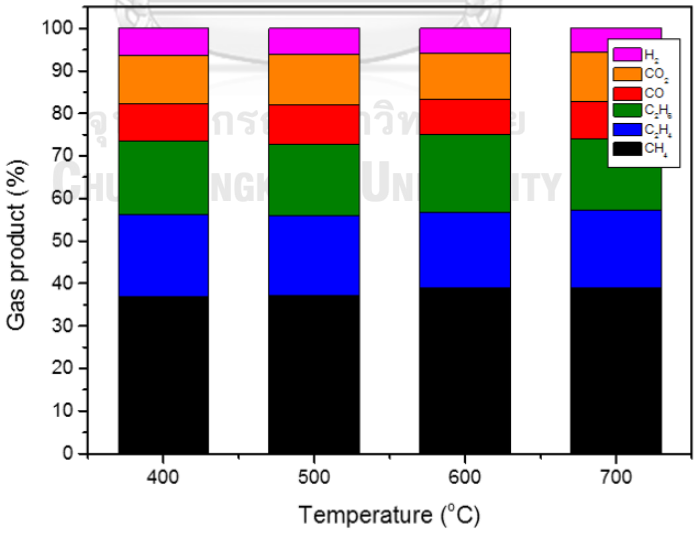

Figure D.2 Effect of carbonization temperature on gas product compositions

D.2 Product compositions obtained from the KOH-activation process

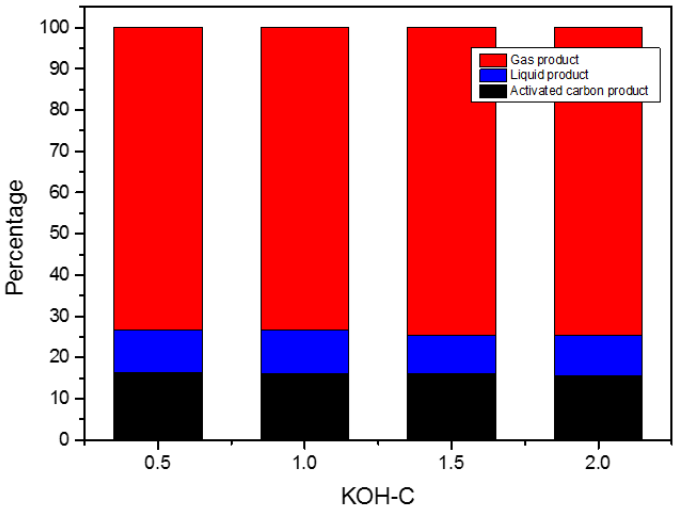

Figure D.3 Effect of activating agent ratio on product compositions
Liquid product: Moisture and Tar

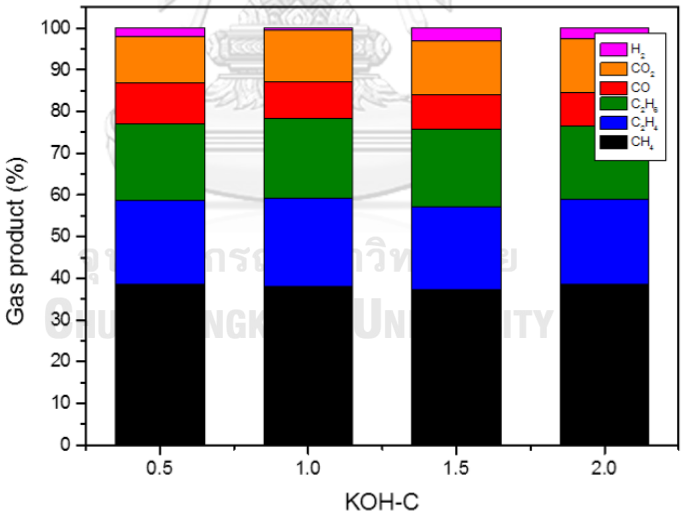

Figure D.4 Effect of activating agent ratio on gas product compositions

D.3 Product compositions obtained from the hydrodeoxygenation (HDO) reaction

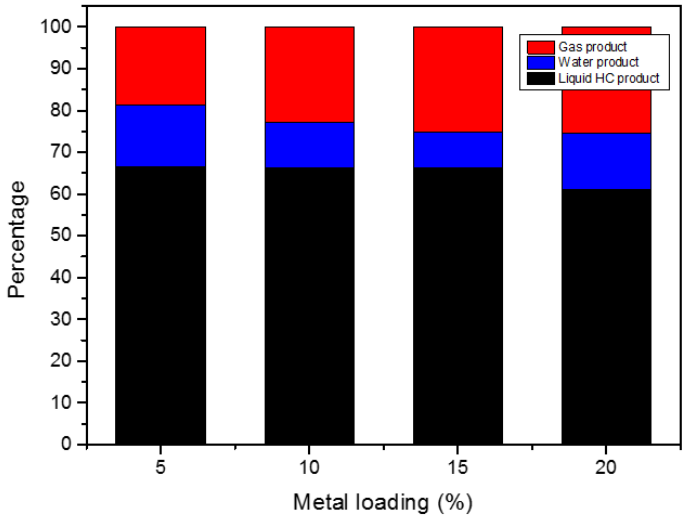

Figure D.5 Effect of molybdenum phosphide loading on product compositions of MoP-AC catalysts with reaction temperature of (a) 400, (b) 420 and (c) 440 °C

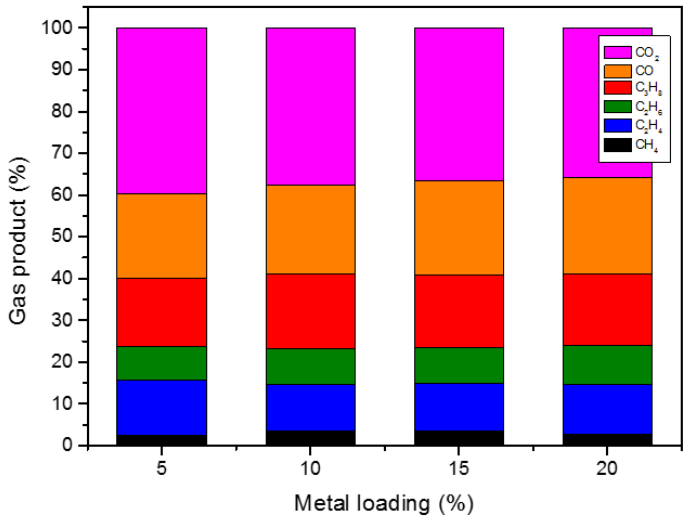

Figure D.6 Effect of molybdenum phosphide loading on gas product compositions of MoP-AC catalysts with reaction temperature of (a) 400, (b) 420 and (c) 440 °C

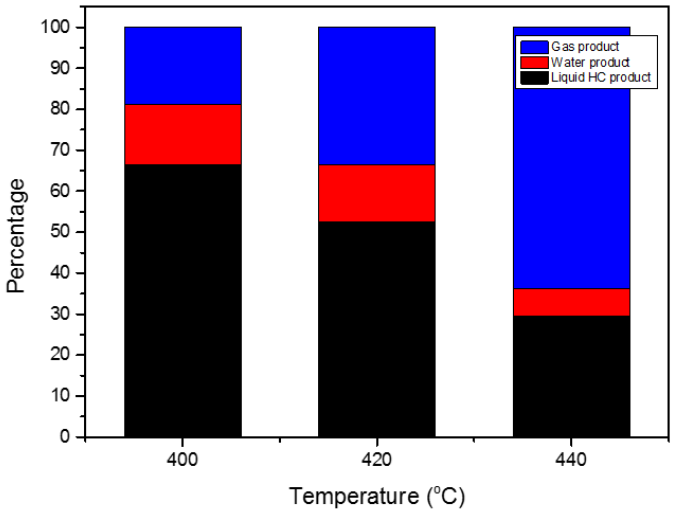

Figure D.7 Effect of reaction temperature on product compositions of 5MoP-AC

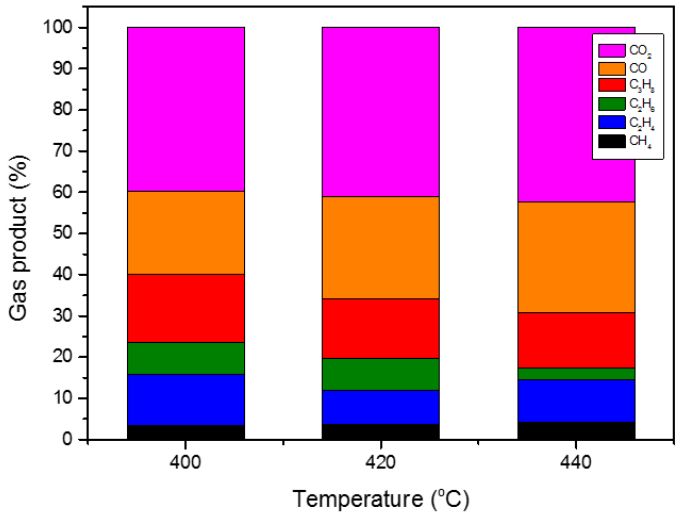

Figure D.8 Effect of reaction temperature on gas product compositions of 5MoP-AC